8 Radiative transfer in horizontally and vertically inhomogeneous turbid media

O. V. Nikolaeva, L. P. Bass, T. A. Germogenova, V. S. Kuznetsov,
A. A. Kokhanovsky

8.1 Introduction

Radiative transfer through turbid media is usually modeled on the basis of the stationary radiative transfer equation (RTE). As a rule, in addition various approximations of the radiative transfer equation, such as the spherical harmonics equations or small angle approximations, are used. The spherical harmonics equations are relevant for transport problems in optically thick and weakly heterogeneous media, whereas small angle approximation works well for radiation transfer problems in media characterized by the phase functions peaked in the forward scattering direction.

Modern methods of atmospheric research require multiply scattered radiation field intensity calculations at large discrete spatial-angular arrays for detailed modeling of light scattering media. Besides, radiation field calculations in the wide range of wavelengths are necessary to estimate solar radiation influence on weather and climate variations. In some cases, however, the information on the scattered radiation field for few wavelengths is sufficient.

So we shall consider the radiative transfer equation for the fixed wavelength value, rather than one for a spectral line. RTE for the radiance $\psi(\vec{r},\vec{\Omega})$ can be written in the form

$$\hat{L}\psi = B(\vec{r},\vec{\Omega})\,, \quad B(\vec{r},\vec{\Omega}) = \hat{S}\psi(\vec{r},\vec{\Omega}) + F(\vec{r},\vec{\Omega})\,, \tag{8.1}$$

where

$$\vec{L}\psi = \vec{\Omega}\cdot\vec{\nabla}\psi(\vec{r},\vec{\Omega}) + K_{\rm ext}(\vec{r})\psi(\vec{r},\vec{\Omega}) \tag{8.2}$$

is a differential transport operator,

$$\hat{S}\psi = K_{\rm ext}(\vec{r})\,\bar{\omega}_0(\vec{r})\int_{-1}^{+1}{\rm d}\gamma\int_0^{2\pi}{\rm d}\varphi\,p(\vec{r},\vec{\Omega}\vec{\Omega}')\,\psi(\vec{r},\vec{\Omega}') \tag{8.3}$$

is an integral operator of scattering, $\vec{\Omega}$ is the direction of propagation, defined by azimuth angle φ and value $\gamma = \cos\theta$, where θ is polar angle (see Fig. 8.1).

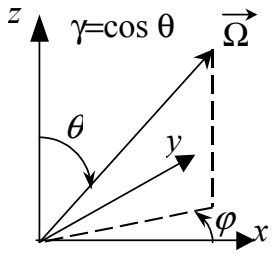

Fig. 8.1. Vector $\vec{\Omega}$.

The extinction coefficient $K_{\rm ext}(\vec{r})$, the single scattering albedo $\bar{\omega}_0(\vec{r})$ and the scattering phase function $p(\vec{r},\chi)$ are suggested to be positive. The following normalization condition for the scattering phase function $p(\vec{r},\chi)$ is used:

$$\int_{-1}^{+1}\int_{0}^{2\pi} {\rm d}\gamma\,{\rm d}\varphi\, p(\vec{r},\vec{\Omega}\cdot\vec{\Omega}') = 1\,, \tag{8.4}$$

where $\chi = \vec{\Omega}\cdot\vec{\Omega}'$ is the inner product of vectors $\vec{\Omega}(\gamma,\varphi)$ and $\vec{\Omega}'(\gamma',\varphi')$,

$$\vec{\Omega}\cdot\vec{\Omega}' = \gamma\,\gamma' + \sqrt{1-\gamma^2}\,\sqrt{1-(\gamma')^2}\,\cos(\varphi-\varphi')\,. \tag{8.5}$$

The function $F(\vec{r},\vec{\Omega})$ defines solar and heat radiation sources. For formulation of a transport problem in the atmospheric region G with the boundary Γ, some boundary conditions on Γ should be also defined:

$$\psi(\vec{r},\vec{\Omega}) = \overline{\psi}(\vec{r},\vec{\Omega}) = A(\vec{r})\,\widehat{R}\,\psi(\vec{r},\vec{\Omega}) + \psi_0(\vec{r},\vec{\Omega})\,, \quad \text{at } \vec{r}\in\Gamma,\ \vec{\Omega}\cdot\vec{n}(\vec{r}) < 0\,. \tag{8.6}$$

Here $\vec{n}(\vec{r})$ is the external normal at the point $\vec{r}$ of the boundary surface Γ and the function $\overline{\psi}(\vec{r},\vec{\Omega})$ defines the radiation intensity entering the region G, $\psi_0(\vec{r},\vec{\Omega})$ is radiation intensity of the source on the boundary surface, $A(\vec{r}) \in [0,1]$ is the reflection albedo. The operator $\widehat{R}$, defining the radiation reflection for the surface Γ, can be written as

$$\widehat{R}\,\psi(\vec{r},\vec{\Omega}) = \int_{\vec{\Omega}'\cdot\vec{n}>0} {\rm Re}\,(\vec{r},\vec{\Omega},\vec{\Omega}')\psi(\vec{r},\vec{\Omega}')\,{\rm d}\vec{\Omega}'\,,$$

${\rm Re}\,(\vec{r},\vec{\Omega},\vec{\Omega}')$ is the bi-directional surface reflectance, normalized by equality

$$\widehat{R}\,[1] = \int_{\vec{\Omega}'\cdot\vec{n}>0} {\rm Re}\,(\vec{r},\vec{\Omega},\vec{\Omega}')\,{\rm d}\vec{\Omega}' = 1\,.$$

In particular, the operator

$$\hat{R}\,\psi(\vec{r},\vec{\Omega}) = \frac{1}{\int_{(\vec{\Omega}'\cdot\vec{n})>0}(\vec{\Omega}'\cdot\vec{n})\,{\rm d}\vec{\Omega}'}\int_{(\vec{\Omega}'\cdot\vec{n})>0}(\vec{\Omega}'\cdot\vec{n})\,\psi(\vec{r},\vec{\Omega}')\,{\rm d}\vec{\Omega}'$$

corresponds to the well known Lambert reflection law, the operator $\hat{R}\,\psi(\vec{r},\vec{\Omega}) = \psi(\vec{r},\vec{\Omega}^*)$ defines mirror reflection processes (here the function $\vec{\Omega}^*(\vec{r},\vec{\Omega})$ defines

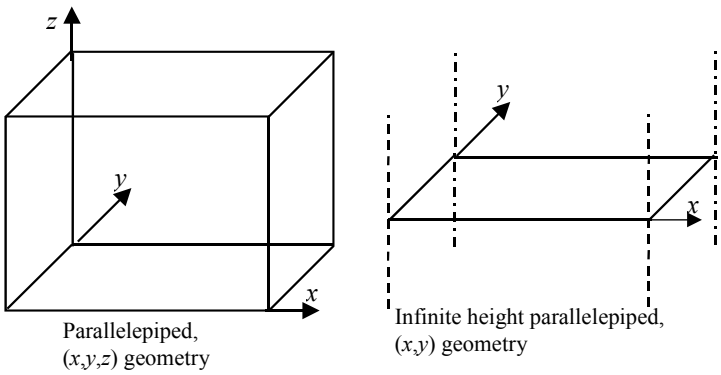

Fig. 8.2. Calculation regions with Cartesian coordinate systems.

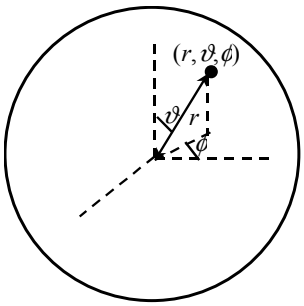

Fig. 8.3. Calculation region with the spherical coordinates system.

vector $\vec{\Omega}^*$, symmetrical to vector $\vec{\Omega}$ relatively the plane perpendicular to surface Γ at the point $\vec{r}$), whereas the operator $\hat{R}\,\psi(\vec{r},\vec{\Omega}) = \psi(\vec{r},-\vec{\Omega})$ corresponds to the returned scattering law, relevant for irregular surfaces.

A parallelepiped is used as a calculation region G in many cases, and so three coordinates $\{x, y, z\}$ define the vector $\vec{r}$ introduced above. Obviously, it is the case of (x, y, z)-geometry, depicted in Fig. 8.2.

More rarely the spherical coordinates $\vec{r} = \{r, \vartheta, \varphi\}$ are used (see Fig. 8.3). There exist situations, when the solution $\psi(\vec{r},\vec{\Omega})$ is independent on one of the variables. Then the corresponding variable is vanished (see Fig. 8.2).

Numerical algorithms for transport equation solving are frequently based either on the stochastic Monte–Carlo (MC) method (Marchuk et al., 1980) or the deterministic Discrete Ordinates Method (DOM) (Chandrasekhar, 1950; Bass et al., 1986). These two methods usually complement each other, each possessing some advantages and shortcomings.

The MC method can easily allow us to take into account the complicated spatial structure of calculation regions. However, it provides solutions of the numerical transport problems only for a small number of radiation detectors. But, as is clear, the smaller detector array size in phase space $\{\vec{r}, \vec{\Omega}\}$ the less the accuracy of calculation of the functional, corresponding to the detector.

Obviously, the smaller the detector size the fewer photons it receives. So, in optically thick media (thick clouds or twilight atmosphere), a large number of histories is necessary. A more complicated way of region nonhomogeneity accounting is used in the DOM method compared to the MC method. However, DOM provides the solution in the whole spatially-angular grid located inside the calculation region, independently of the region size. Test calculations confirm high DOM accuracy even in the case when the solution undergoes variations over 18–20 orders. On the other hand, due to the necessity of radiation field calculation in the whole region, DOM is sometimes proved more computationally expensive as compared to the MC method.

The slab model approximation is relevant for radiation transfer problems in horizontally homogeneous regions (such as a cloud or clear sky). If slab optical thickness is more than 5–8 optical lengths, asymptotic methods may be used for reflected and transferred light intensity calculations. For complicated radiation transport problems, various decomposition techniques have been developed, consisting of combinations of analytical, asymptotic and simple numerical methods. The development of multiprocessor computers enables us to increase DOM codes efficiency. Parallel calculation algorithms enable us to decrease DOM calculation time and so to come close to MC, despite the MC itself parallelizing. Besides, the nonhomogeneity approximation accuracy via DOM is currently almost as high as that via the MC method.

Below we shall consider discrete ordinates methods for the transport equation, namely: the specification of transport equation parameters (section 8.2); the construction of angular (section 8.3) and spatial (section 8.6) grids; the scattering integral $\hat{S}$ (section 8.4) and the differential operator $\hat{L}$ (section 8.6) approximations; and the separation of diffused and direct light (section 8.5). In correspondence with the introduced classification (section 8.6) various grids schemes will be considered (sections 8.7–8.10), methods of grid equations will be presented (section 8.11) and parallel calculation organization will be introduced (section 8.12). Code implementations of various DOM versions for atmosphere optics problems will be given in sections 8.13 and 8.14.

8.2 Description of the calculation region

We present results of radiation field calculations in a cloudy atmosphere on the set of pixels. Each pixel size (on the (x, y) plane) corresponds to the required calculation accuracy, vertical atmosphere characteristics (over z-axis) being considered as known. An example of the representation of atmosphere by 3.6×10^5 pixels is given by Cahalan et al. (2005).

In each pixel, the transfer equation coefficient behavior over the height (z-axis) is suggested to be known (via the direct problem solution). The spatial grid mesh in the calculation region cannot be larger than the corresponding pixel size.

Proper approximations for cross-sections of aerosol and molecular light scattering processes and light absorption by various gases are used in transport problems. Corresponding coefficients in the transport equation are then obtained as

weighted mean values over aerosol, molecular, gaseous and cloudy contributions. For example, for a cloud consisting of water (w) and ice (i), transport equation coefficients are defined by formulas

$$K_{\rm ext} = K_{ext,w} + K_{ext,i}\,, \quad \omega_0 = \frac{\omega_{0,w} K_{ext,w} + \omega_{0,i}\, K_{ext,i}}{K_{ext,w} + K_{ext,i}}\,,$$

$$p = \frac{\omega_{0,w} K_{ext,w} p_w + \omega_{0,i} K_{ext,i} p_i}{\omega_{0,w} K_{ext,w} + \omega_{0,i} K_{ext,i}}\,.$$

These coefficients are usually approximated by constants either inside the pixel or inside the spatial grid mesh.

8.3 Discrete ordinates method and a angular quadratures

The discrete ordinates method is based on the transfer from the continuous angular dependence of the transport equation solution to the discrete one, that is on the introduction of the angular quadrature over variables θ and φ on the unit sphere $\{-1 < \gamma < 1,\ 0 < \varphi < 2\pi\}$.

Let us consider such a quadrature for the hemisphere $\{-1 < \gamma < 1, 0 < \varphi < \pi\}$. At first, the interval $-1 < \gamma < 1$ is divided into subintervals

$$\begin{aligned} -1 &= \gamma_{-L-1/2} < \cdots < \gamma_{-\ell-1/2} < \ldots \gamma_{-1/2} \\ &= 0 = \gamma_{1/2} < \cdots < \gamma_{\ell+1/2} < \ldots \gamma_{L+1/2} = 1 \end{aligned}$$

with nodes γ_ℓ, $\ell = 1, \ldots, L$, being chosen inside each subinterval:

$$\gamma_\ell \in [\gamma_{\ell-1/2}, \quad \gamma_{\ell+1/2}]\,, \quad \gamma_{-\ell} \in [\gamma_{-\ell-1/2},\ \gamma_{-\ell+1/2}]\,, \quad \Delta\gamma_\ell = \left|\gamma_{\ell+1/2} - \gamma_{\ell-1/2}\right|\,.$$

A similar subdivision of interval $0 < \varphi < \pi$ is introduced for each node γ_ℓ:

$$0 = \varphi_{\ell,1/2} < \cdots < \varphi_{\ell,m+1/2} < \cdots < \varphi_{\ell,M_\ell+1/2} = \pi\,,$$

$$\Delta\varphi_{\ell,m} = \varphi_{\ell\,,m+1/2} - \varphi_{\ell,m-1/2}\,, \quad \varphi_{\ell,m} \in (\varphi_{\ell\,,m-1/2},\ \varphi_{\ell,m+1/2})\,.$$

Thus, the hemisphere is decomposed into the set of fragments, each point $\{\gamma_\ell, \varphi_{\ell,m}\}$ being chosen as a quadrature node, with the value of a hemisphere element $w_{\ell,m} = \Delta\gamma_\ell\, \Delta\varphi_{\ell,m}$ being equal to corresponding quadrature weight. Similarly, the quadrature can be introduced for another hemisphere.

The quadrature is called a *rectangular* one if the number M_ℓ of subintervals over φ is the same for each γ-layer. Concentration of nodes near the unit sphere poles represents the main shortcoming of the rectangular quadrature. There is not this shortcoming in triangular quadratures: the closer node γ_ℓ is to the sphere pole the less the corresponding parameter M_ℓ.

Two important requirements should be satisfied for the quadrature construction. The first requirement is that quadrature nodes should be distributed in a maximally uniform manner over the unit sphere. The second one is that the quadrature should provide an exact calculation of the following integrals:

$$\sum_{\ell=1}^{2L} \gamma_\ell^{k_1}\, \Delta\gamma_\ell = \int_{-1}^{1} \mathrm{d}\gamma\, \gamma^{k_1}\,, \tag{8.7a}$$

$$\sum_{\ell=1}^{2L} \Delta\gamma_\ell \sum_{m=1}^{M_\ell} \xi_{\ell,m}^{k_2} \Delta\varphi_{\ell,m} = \int_{-1}^{1} \mathrm{d}\gamma \int_0^{\pi} \mathrm{d}\varphi \xi^{k_2}(\gamma,\varphi)\,, \tag{8.7b}$$

$$\sum_{\ell=1}^{2L} \Delta\gamma_\ell \sum_{m=1}^{M_\ell} \eta_{\ell,m}^{k_3} \Delta\varphi_{\ell,m} = \int_{-1}^{1} \mathrm{d}\gamma \int_0^{\pi} \mathrm{d}\varphi \eta^{k_3}(\gamma,\varphi)\,, \tag{8.7c}$$

where the set of values k_1, k_2, k_3 depends on quadrature type. Here the values ξ, η, γ are projections of transport vector $\vec{\Omega}$ on coordinate axes x, y and z, correspondingly, see Fig. 8.1:

$$\xi_{\ell,m} = \xi(\gamma_\ell, \varphi_{\ell,m}),\ \eta_{\ell,m} = \eta(\gamma_\ell, \varphi_{\ell,m}),\ \xi = \sin\theta\cos\varphi,\ \eta = \sin\theta\sin\varphi,\ \gamma = \cos\theta\,.$$

The scattering integral in the transfer equation can be calculated with a high accuracy, if Eqs (8.7a)–(8.7c) are satisfied.

Two examples of the triangular angular quadrature with $M_\ell = 2(L - |\ell| + 1)$ are depicted in Fig. 8.4. Here the darker shading is prescribed for the larger sphere fragment.

Although the distribution of *LQ-quadrature* nodes over the sphere is not uniform (see Fig. 8.4), the quadrature is symmetrical with respect to rotation by 90°. Besides, it satisfies the conditions (8.7) at $k = 0, 1, \ldots, 2L$. Unfortunately, these useful quadratures exist only for $L \le 10$, because equations, defining weights and nodes of the LQ-quadarature, are not resolved at $L > 10$.

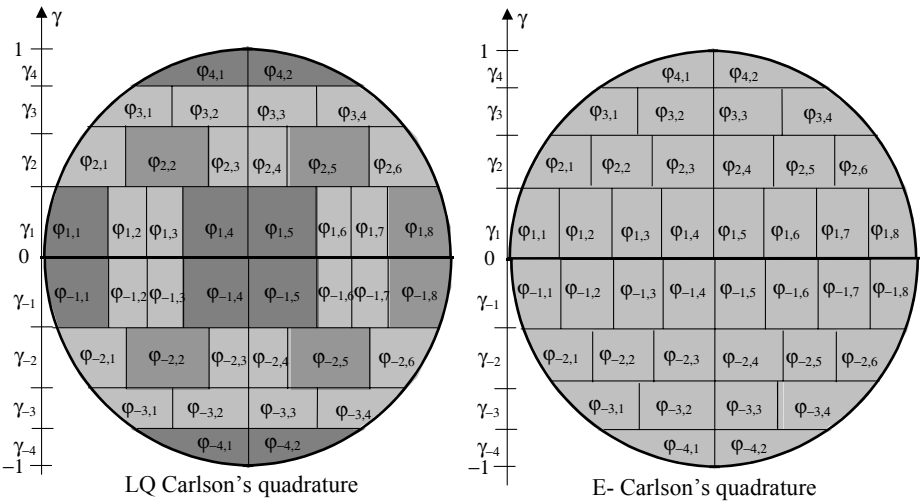

Fig. 8.4. Examples of angular quadratures for hemisphere $\{-1 < \gamma < 1,\ 0 < \varphi < \pi\}$.

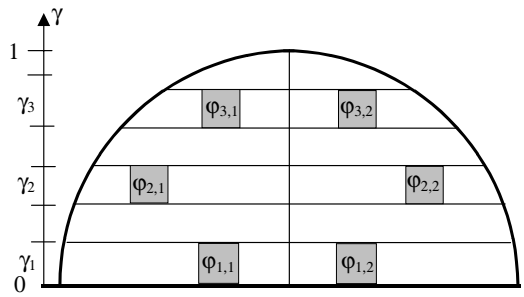

Fig. 8.5. Six nodes of one set for DCT quadrature.

E-quadrature (Carlson, 1976) exists for arbitrary L. All squares $w_{\ell,m}$ of the quadrature are equal to value $\pi/(L\,(L+1))$, see Fig. 8.4. Such severe constraint does not provide great freedom for quadrature node choice, because Eqs (8.7a)–8.7c) are exactly satisfied only for $k = 0, 1, 2$ in the case of E-quadrature.

DCT (double circle triangle) quadratures (Koch et al., 1995) are generalization of Carlson's ones. DCT grids consist of sets, each of which contains six nodes arranged on one quadrant; see an example in Fig. 8.5. Weights of all six nodes must be identical. This ensures the quadrature symmetry. But weights of different sets may be chosen differently that provide free parameters to increase the quadrature accuracy in the sense of Eq. (8.7).

Equation (8.7a) for $k = 0, 1, \ldots, 4L-1$ is satisfied in the case of *Gauss's grid* over γ. If one uses a uniform φ-grid with centered nodes for each γ-layer (i.e. at $\varphi_{\ell,m} = (\varphi_{\ell,m+1/2} + \varphi_{\ell,m-1/2})/2$), then conditions (8.7b) and (8.7c) are approximately satisfied (the accuracy being sufficiently high for a large number of quadrature nodes). The conditions (8.7b) and (8.7c) are exactly fulfilled for the Gaussian φ-grid. However, in this case the node distribution is inhomogeneous. It should be noted that another interpolation formulas can be used instead of those based on Gaussian grid. For example, one can use either *Radau quadrature* (where $\gamma_{-L} = -1$, and the condition (8.7a) is fulfilled for $k = 0, 1, \ldots, 4L-2$) or *Lobatto quadrature* (where $\gamma_{-L} = -1$, $\gamma_L = 1$, and the condition (8.7a) is satisfied for $k = 0, 1, \ldots, 4L-3$).

The quadratures with weights and nodes that permit exact integration of polynomials up to the highest possible order and are invariant to the desired rotation group have features of both Gauss's and Carlson's grids (Lebedev, 1976). The weights and nodes of these quadratures are defined by non-linear algebraic systems.

The significant shortcoming of all mentioned quadratures is that the grid condensing cannot be realized uniformly as L increases. That is to say, each fragment of a coarser grid is not formed by proper combination of fragments of a finer grid. A *Special T-quadrature* (Aussourd, 2003) is constructed, where this problem is solved: each portion of a coarser grid is divided into four identical portions of a finer grid (an example is shown in Fig. 8.6).

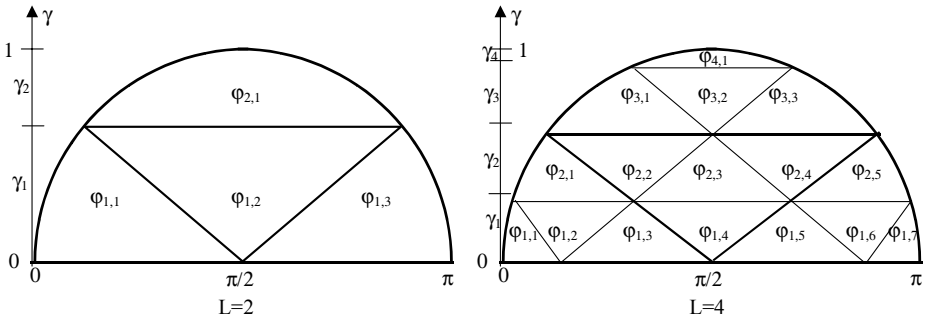

Fig. 8.6. T-quadrature for $\{0 < \gamma < 1,\ 0 < \varphi < \pi\}$.

The mentioned feature of the T-quadrature provides the capability to condense (refine) the angular grid in that solid angle, where the transport equation solution significantly depends on angular variables. Additional nodes are then simply added to the initial quadrature grid, whereas using other quadratures one has to correct the neighboring nodes in the process of grid condensing to keep Eqs (8.7) fulfillment for a finer grid (Longoni and Haghighat, 2001).

For problems with the forward peaked phase functions, common for atmospheric optics problems, special kinds of quadratures were constructed, for which quadrature nodes are concentrated near sphere poles (Sanchez and McCormic, 2004).

8.4 Scattering integral representation

After the introduction of angular quadratures in DOM, the solution $\psi(\vec{r}, \gamma, \varphi)$ is replaced by a collection of functions $\psi(\vec{r}, \gamma_\ell, \varphi_{\ell,m})$. Two types of the scattering integral $\hat{S}\psi$ representations exist. The first type is widely used in neutron physics and atmospheric optics problems. Here the phase function $p(\vec{r}, \vec{\Omega}\cdot\vec{\Omega}')$ is presented via expansion into a finite sum on the Legendre polynomials,

$$p(\vec{r}, \vec{\Omega}\cdot\vec{\Omega}') = \frac{1}{4\pi}\sum_{\nu=1}^{N(\vec{r})}(2\nu+1)\,\omega_\nu(\vec{r})\,P_\nu(\vec{\Omega}\cdot\vec{\Omega}')\,, \tag{8.8}$$

that are orthogonal in the interval $(-1,\,1)$:

$$\int_{-1}^{1} P_n(\chi)\,P_\nu(\chi)\,\mathrm{d}\chi = 2\,\delta_{n,\nu}/(2n+1)\,,$$

where $\delta_{n,\nu}$ is the Kronecker delta symbol. The expansion coefficients are defined by formulas

$$\omega_\nu(\vec{r}) = 2\,\pi\int_{-1}^{1} p(\vec{r},\chi)\,P_\nu(\chi)\,\mathrm{d}\chi\,, \quad \omega_0(\vec{r}) \equiv 1\,. \tag{8.9}$$

The expression (8.5) and Legendre polynomials adding theorem (Ryzik and Gradstein, 1972)

$$P_\nu(\vec{\Omega}\,\vec{\Omega}') = P_\nu^0(\gamma)\,P_\nu^0(\gamma') + 2\sum_{\mu=1}^{\nu}\frac{(\nu-\mu)!}{(\nu+\mu)!}P_\nu^\mu(\gamma)\,P_\nu^\mu(\gamma')\,\cos\mu\,(\varphi-\varphi')\,,$$

where

$$P_\nu^\mu(\gamma) = (-1)^\mu\,(1-\gamma^2)^{\mu/2}\,\frac{\mathrm{d}^\mu}{\mathrm{d}\gamma^\mu}\,P_\nu(\gamma)$$

are the associated Legendre functions, allow us to represent the scattering integral $\hat{S}\psi$ by the following sum

$$\begin{aligned}\hat{S}\psi \;=\; & \frac{1}{4\pi}K_{\mathrm{ext}}(\vec{r})\,\bar{\omega}_0(\vec{r})\sum_{\nu=0}^{N(\vec{r})}(2\nu+1)\,\omega_\nu(\vec{r})\left\{P_\nu^0(\gamma)\,M_{\nu,0}^c(\vec{r})\right.\\ & \left.+\,2\sum_{\mu=1}^{\nu}\frac{(\nu-\mu)!}{(\nu+\mu)!}P_\nu^\mu(\gamma)\cdot\left[\cos\mu\varphi\,M_{\nu,\mu}^c(\vec{r})+\sin\mu\varphi\,M_{\nu,\mu}^s(\vec{r})\right]\right\},\quad(8.10)\end{aligned}$$

where angular moments $M_{\nu,\mu}^c(\vec{r})$ and $M_{\nu,\mu}^s(\vec{r})$ of the solution are determined as

$$M_{\nu,\mu}^c(\vec{r}) = \int_{-1}^{1}\mathrm{d}\gamma\int_0^{2\pi}P_\nu^\mu(\gamma)\,\cos\mu\varphi\,\psi(\vec{r},\gamma,\varphi)\,\mathrm{d}\varphi\,,$$

$$M_{\nu,\mu}^s(\vec{r}) = \int_{-1}^{1}\mathrm{d}\gamma\int_0^{2\pi}P_\nu^\mu(\gamma)\,\sin\mu\varphi\,\psi(\vec{r},\gamma,\varphi)\,\mathrm{d}\varphi\,.$$

After replacing all integrals by corresponding quadrature sums

$$\begin{aligned}M_{\nu,\mu}^c(\vec{r}) \;&\simeq\; \sum_\ell\sum_m P_\nu^\mu(\gamma_\ell)\,\cos\mu\varphi_{\ell,m}\,\psi(\vec{r},\gamma_\ell,\varphi_{\ell,m})\,,\\ M_{\nu,\mu}^s(\vec{r}) \;&\simeq\; \sum_\ell\sum_m P_\nu^\mu(\gamma_\ell)\,\sin\mu\varphi_{\ell,m}\,\psi(\vec{r},\gamma_\ell,\varphi_{\ell,m})\,,\end{aligned}\qquad(8.11)$$

we obtain the discrete representation of the scattering integral.

Utilizing representation (8.10), one can store a set of angular moments (8.11) and values $P_\nu^\mu(\gamma_\ell)\,\cos\mu\varphi_{\ell,m}$ and $P_\nu^\mu(\gamma_\ell)\,\sin\mu\varphi_{\ell,m}$ in computer memory, rather than solution values at grid nodes.

The second type of the integral $\hat{S}\psi$ representation consists in the direct replacement of $\hat{S}\psi$ by quadrature sums:

$$\hat{S}\psi(\vec{r},\gamma_\ell,\varphi_{\ell,m}) \simeq K_{\mathrm{ext}}\bar{\omega}_0(\vec{r})\sum_{\ell'}\sum_{m'}H_{\ell,\ell',m,m'}(\vec{r})\,\psi(\vec{r},\gamma_{\ell'},\varphi_{\ell',m'})\,w_{\ell',m'}\,,$$

$$H_{\ell,\ell',m,m'}(\vec{r}) \approx p\left(\vec{r},\gamma_\ell\,\gamma_{\ell'}+\sqrt{1-\gamma_\ell^2}\,\sqrt{1-(\gamma_{\ell'})^2}\cos(\varphi_{\ell,m}-\varphi_{\ell',m'})\right),$$

and normalization conditions (see (8.4)) must be kept

$$\sum_{\ell'} \sum_{m'} H_{\ell,\ell',m,m'}(\vec{r})\, w_{\ell',m'} = 1\,.$$

Now the values $\psi(\vec{r}, \gamma_\ell, \varphi_{\ell,m})$ themselves and the elements of the scattering matrix H should be stored in computer memory during calculations. It is noteworthy that the number $\tilde{N}(\vec{r})$ of angular moments (8.11), which form the solution accordingly to formula (8.10), is equal to $[N(\vec{r})]^2$, where $N(\vec{r})$ is the number of moments used for the phase function representation (see Eq. (8.8)). If the solution is an even function of the azimuth angle φ, the moments $M^s_{\nu,\mu}(\vec{r})$ vanish, and so only $\tilde{N}(\vec{r}) = N(\vec{r})\,[N(\vec{r}) + 1]/2$ moments are used in calculations.

Thus, while using the first method, one should store $\tilde{N}(\vec{r})\,(1 + 2M)$ values (angular moments and auxiliary values $P^\mu_\nu(\gamma_\ell)\cos\mu\varphi_{\ell,m}$, $P^\mu_\nu(\gamma_\ell)\sin\mu\varphi_{\ell,m}$) for each spatial mesh $\vec{r}$, whereas in the case of using the second method, exactly $M + M^2$ values (solution results and scattering matrix elements) should be stored (here M is full number of quadrature nodes). So, as one can see, the first method requires less computer memory than the second one, if $\tilde{N}(\vec{r}) < M\,(M + 1)/(2M + 1)$. The last inequality is valid in the case of reactor-shielding problems, where $N(\vec{r}) \le 5$, $M \le 80$. The phase functions are of more complex type in problems of radiation transfer through the terrestrial atmosphere, and therefore one should use the sums of a great number of Legendre polynomials to represent them. Hence the second method can be more economic because it uses a smaller number of quadrature nodes. Note also, that matrix elements $H_{\ell,\ell',m,m'}(\vec{r})$ may be calculated during the main computation procedure, rather than stored in computer memory. It will result in a decrease in the necessary memory volume, but an increase in the calculation time.

It is just the first method that is applied in the majority of codes using the scattering integral calculation. The associated Legendre functions $P^\mu_\nu(\gamma)$ are usually calculated via the recurrent formulas (Ryzik and Gradstein, 1972):

$$P^\mu_{\nu+1}(\gamma) = \frac{2\nu+1}{\nu-\mu+1}\,\gamma\,P^\mu_\nu(\gamma) - \frac{\nu+\mu}{\nu-\mu+1}\,P^\mu_{\nu-1}(\gamma)\,, \tag{8.12}$$

where

$$\begin{aligned} P^\nu_\nu(\gamma) &= \left(1-\gamma^2\right)^{\nu/2}\,(-1)^\nu\,\frac{(2\nu)!}{2^\nu\nu!}\,, \\ P^{\nu-1}_\nu(\gamma) &= \gamma\,\left(1-\gamma^2\right)^{(\nu-1)/2}\,(-1)^{\nu-1}\,\frac{(2\nu-1)!}{2^{\nu-1}\,(\nu-1)!}\,. \end{aligned}$$

In atmospheric optics transport problems, one has often to deal with highly forward-peaked phase functions, defined via values at the nodes of a some grid over the scattering angle χ. The calculation of coefficients $\omega_\nu(\vec{r})$ in the expansion (8.8) represents a complicated problem for such phase functions at $\nu > 60$, because of two facts:

(a) the Legendre polynomials of high order, contained in the integrals (8.9), are quickly oscillating functions, especially in the vicinity of points $\chi = \pm 1$,

(b) the Legendre polynomial values are incorrectly calculated near $\chi = \pm 1$ (see Eq. (8.12)). A widely used code, presented at the site http://rts.kiam.ru/verval/sfxp.htm, is based on a special approach for effective $\omega_\nu(\vec{r})$ calculations with a high accuracy.

An adequate representation of highly forward-peaked phase functions requires calculations with a large number of polynomials (up to some hundreds and even thousands). For this reason, it is helpful to decompose a highly-peaked phase function into the sum of a singular component (corresponding to the phase function peak) and a regular component. The expansion (8.8) can be applied to the regular component only, the singular component being approximated by the delta-function (Wiscombe, 1977; Landesman and Morel, 1989).

8.5 The general solution

As was mentioned in the introduction, function $F(\vec{r}, \vec{\Omega})$ in Eq. (8.1) describes radiation sources, usually representing either solar or thermal radiation. In the first case function $F(\vec{r}, \vec{\Omega})$ is singular with respect to angular variables:

$$F(\vec{r}, \vec{\Omega}) = F_0 \, \delta(\vec{\Omega} - \vec{\Omega}_0) \, \delta(f_0(\vec{r})) \,,$$

where δ is the Dirac delta-function, the vector $\vec{\Omega}_0$ defines the solar radiation direction, F_0 is the solar radiation flux and the function $f_0(\vec{r})$ determines the surface through which radiation penetrates into the region under consideration.

The solution can be presented as the sum of two functions

$$\psi(\vec{r}, \vec{\Omega}) = \psi_n(\vec{r}, \vec{\Omega}) + \psi_s(\vec{r}, \vec{\Omega}) \,,$$

function-terms being the solutions to the following problems

$$\hat{L}\psi_n(\vec{r}, \vec{\Omega}) = F(\vec{r}, \vec{\Omega}) \,, \quad \psi_n(\vec{r}, \vec{\Omega}) = 0 \,, \quad \text{as } \vec{r} \in \Gamma, \ \vec{\Omega} \cdot \vec{n}(\vec{r}) < 0 \tag{8.13}$$

and

$$\hat{L}\psi_s(\vec{r}, \vec{\Omega}) = \hat{S}\psi_s(\vec{r}, \vec{\Omega}) + \hat{S}\psi_n(\vec{r}, \vec{\Omega}) \,,$$

$$\psi_s(\vec{r}, \vec{\Omega}) = A(\vec{r}) \, \widehat{R} \, \psi_s(\vec{r}, \vec{\Omega}) + A(\vec{r}) \, \widehat{R} \, \psi_n(\vec{r}, \vec{\Omega}) + \varphi_0(\vec{r}, \vec{\Omega}) \quad \text{as } \vec{r} \in \Gamma, \vec{\Omega} \cdot \vec{n}(\vec{r}) < 0 \,.$$

Here the function $\psi_n(\vec{r}, \vec{\Omega})$ corresponds to the unscattered component of radiation, whereas the function $\psi_s(\vec{r}, \vec{\Omega})$ represents the scattered component. The problem (8.13) for the unscattered component can be easily solved analytically, whereas the scattered component $\psi_s(\vec{r}, \vec{\Omega})$ has to be obtained numerically with the help a grid scheme.

8.6 Approximation of differential operator $\hat{L}$

When grid approximations of operator $\hat{L}$ are performed, the function $B(\vec{r}, \vec{\Omega})$ in Eq. (8.1) and the boundary source $\overline{\psi}(\vec{r}, \vec{\Omega})$ are assumed to be known (further indices ℓ, m in all formulas are omitted). At the first step, the spatial grid itself is specified. For example, in the case of (x, y, z) geometry we have

$$\begin{aligned} &x_{1/2} < \ldots < x_{i+1/2} < \ldots < x_{I-1/2} < x_{I+1/2}\,, \\ &y_{1/2} < \ldots < y_{j+1/2} < \ldots < y_{J-1/2} < y_{J+1/2}\,, \\ &z_{1/2} < \ldots < z_{k+1/2} < \ldots < z_{K-1/2} < z_{K+1/2}\,. \end{aligned} \tag{8.14}$$

Here $x_{i\pm1/2}, y_{j\pm1/2}, z_{k\pm1/2}$ are grid mesh bounds,

$$\Delta x_i = x_{i+1/2} - x_{i-1/2}\,, \quad \Delta y_i = y_{j+1/2} - y_{j-1/2}\,, \quad \Delta z_k = z_{k+1/2} - z_{k-1/2}$$

are mesh sizes,

$$x_i = (x_{i+1/2} + x_{i-1/2})/2\,, \;\; y_j = (y_{j+1/2} + y_{j-1/2})/2\,, \;\; z_k = (z_{k+1/2} + z_{k-1/2})/2$$

are mesh centers, and integer I, J, K are numbers of meshes.

Each grid mesh is a parallelepiped. Algorithms, based on the grids with meshes of tetrahedral or even arbitrary polyhedral forms, have been developed, aimed at accuracy increasing in the representation of discontinuity surfaces for the coefficient of the transport equation (Morel and Larsen, 1990; Castriani and Adams, 1995; Grove and Pevey, 1995). Further, we do not consider the problems related to a design of such complicated grids and corresponding calculations. We consider only regular grids of a type given by Eq. (8.14).

Spatial moments of the solution rather than solution values themselves appear as calculation values at grid nodes. (Remember that *spatial moments* are integrals of the solution over a mesh and its bounds, integration being fulfilled with different weight functions.) For example, for grid (8.14) the *zero spatial moments*, arising in the case when the weight function is equal to 1, are defined by the formulas

$$\begin{aligned} \psi_{i,j,k} &= \frac{1}{\Delta x_i \Delta y_j \Delta z_k} \int_{x_{i-1/2}}^{x_{i+1/2}} \mathrm{d}x \int_{y_{j-1/2}}^{y_{j+1/2}} \mathrm{d}y \int_{z_{k-1/2}}^{z_{k+1/2}} \mathrm{d}z \psi(x, y, z)\,, \\ \psi_{i\pm1/2,j,k} &= \frac{1}{\Delta y_j\, \Delta z_k} \int_{y_{j-1/2}}^{y_{j+1/2}} \mathrm{d}y \int_{z_{k-1/2}}^{z_{k+1/2}} \mathrm{d}z \psi(x_{i\pm1/2}, y, z)\,, \\ \psi_{i,j\pm1/2,k} &= \frac{1}{\Delta x_i\, \Delta z_k} \int_{x_{i-1/2}}^{x_{i+1/2}} \mathrm{d}x \int_{z_{k-1/2}}^{z_{k+1/2}} \mathrm{d}z\, \psi(x, y_{j\pm1/2}, z)\,, \\ \psi_{i,j,k\pm1/2} &= \frac{1}{\Delta x_i\, \Delta y_j} \int_{x_{i-1/2}}^{x_{i+1/2}} \mathrm{d}x \int_{y_{j-1/2}}^{y_{j+1/2}} \mathrm{d}y\, \psi(x, y, z_{k\pm1/2})\,. \end{aligned} \tag{8.15}$$

These values may be interpreted as average values of the solution over a mesh, including its bounds. The averages of the solution are expected to be more stable characteristics of the solution, than solution values themselves at grid nodes.

For moments of a higher order, the polynomials of a corresponding order appear as weight functions. For example, the moments of the first order can be defined by relations

$$\begin{aligned}
\psi^{1,x}_{i,j,k} &= \frac{3}{\Delta x_i \Delta y_j \Delta z_k} \int_{x_{i-1/2}}^{x_{i+1/2}} \mathrm{d}x \bar{P}_1(x) \int_{y_{j-1/2}}^{y_{j+1/2}} \mathrm{d}y \int_{z_{k-1/2}}^{z_{k+1/2}} \mathrm{d}z \psi(x,y,z)\,, \\
\psi^{1,y}_{i,j,k} &= \frac{3}{\Delta x_i \Delta y_j \Delta z_k} \int_{x_{i-1/2}}^{x_{i+1/2}} \mathrm{d}x \int_{y_{j-1/2}}^{y_{j+1/2}} \mathrm{d}y \bar{P}_1(y) \int_{z_{k-1/2}}^{z_{k+1/2}} \mathrm{d}z \psi(x,y,z)\,, \\
\psi^{1,z}_{i,j,k} &= \frac{3}{\Delta x_i \Delta y_j \Delta z_k} \int_{x_{i-1/2}}^{x_{i+1/2}} \mathrm{d}x \int_{y_{j-1/2}}^{y_{j+1/2}} \mathrm{d}y \int_{z_{k-1/2}}^{z_{k+1/2}} \mathrm{d}z \bar{P}_1(z) \psi(x,y,z)\,, \qquad (8.16)
\end{aligned}$$

where

$$\bar{P}_1(x) = \frac{x - x_i}{\Delta x_i/2}\,, \quad \bar{P}_1(y) = \frac{y - y_j}{\Delta y_j/2}\,, \quad \text{and } \bar{P}_1(z) = \frac{z - z_k}{\Delta z_k/2}$$

are the first Legendre polynomial to meshes $[x_{i-1/2},\ x_{i+1/2}]$, $[y_{j-1/2},\ y_{j+1/2}]$ and $[z_{k-1/2},\ z_{k+1/2}]$, correspondingly. They enable us to expand the solution in the spatial mesh $[x_{i-1/2},\ x_{i+1/2}] \times [y_{j-1/2},\ y_{j+1/2}] \times [z_{k-1/2},\ z_{k+1/2}]$ in following manner

$$\begin{aligned}
&\psi(x,y,z) = \psi_{i,j,k} + \bar{P}_1(x)\,\psi^{1,x}_{i,j,k} + \bar{P}_1(y)\,\psi^{1,y}_{i,j,k} + \bar{P}_1(z)\,\psi^{1,z}_{i,j,k} + O(\Delta^2)\,, \\
&\Delta = \max\{\Delta x_i,\ \Delta y_j,\ \Delta z_k\}\ .
\end{aligned}$$

This presentation leads to the nodal grid scheme that is more accurate than schemes based on moments (8.15) and the assumption

$$\psi(x,y,z_k) = \psi_{i,j,k} + O(\Delta)\,.$$

8.6.1 Properties of DOM grid schemes

The *grid scheme accuracy* is of importance in scheme characteristics analysis. For some schemes considered below the following estimations can be obtained:

$$\left\| \vec{\psi}^{\,\mathrm{exact}} - \vec{\psi} \right\| \le C h^q \quad \text{as} \quad h \to 0,\ q = 1, 2, \ldots\,, \qquad (8.17)$$

where the vector $\vec{\psi}$ is formed by grid values of the solution moments, the vector $\vec{\psi}^{\,\mathrm{exact}}$ consists of exact solution moments at corresponding meshes, h is the largest mesh 'diameter' in terms of the optical length, C is a constant, which is independent on h. Usually the constant C is proportional to the greatest absolute value of some derivative from the exact solution $\psi(\vec{r}, \vec{\Omega})$. The norm, figuring in Eq. (8.17), is either the uniform one (being defined by the maximum of the absolute value of the difference $(\vec{\psi}^{\,\mathrm{exact}} - \vec{\psi})$) or the mean square one. The estimation (8.17) means, that the grid solution converges to the exact solution under spatial grid refining. Under condition (8.17) the scheme is said to have qth order of accuracy on the set of smooth solutions.

Surely, the estimations (8.17) are not valid in those sub-regions, where the exact solution has no necessary derivatives. In particular, the exact solution is

not smooth near the surfaces, where coefficients of transport equation are discontinuous (Germogenova, 1985). Besides, spatial grid dimensions are naturally bounded by current computer capabilities, and so calculations cannot be always performed on the basis of grids that are as fine as may be desired. Therefore, it is impossible to be restricted to the accuracy estimations of type (8.17). Qualitative properties of the grid solutions on arbitrary grids are of a significant value. In particular, a quite important moment is that a grid solution should satisfy some *balance relation*, that is a result of the transport equation integration over a spatial mesh and over all directions. It guarantees the conservation of a photon number in the computation process. Significant errors in the grid solution are possible in the case when the balance relation is not satisfied.

Besides, as the computational practice demonstrates, reliable results can be obtained only with the help of schemes, that guarantee the preservation of main qualitative features of exact solutions. The non-negativity of the solution under non-negative sources and the monotonicity of the solution along any characteristics under monotonic effective source $B(\vec{r},\vec{\Omega})/K_{\rm ext}(\vec{r})$ belong to strictly established characteristic features of exact solutions (Bass et al., 1986). The computational schemes, ensuring these essential features of grid solutions, are called *positive* and *monotonic schemes* correspondingly. Calculations with non-positive schemes can result in non-positive grid solutions that should be considered as non-physical (because the function $\psi(\vec{r},\vec{\Omega})$ defines the positive radiance). In addition, grid solutions obtained by means of non-monotonic schemes can have significant non-physical oscillations.

Finally, an additional feature of grid schemes for the transport equation should be noted: the higher the scheme order, the lower the degree of positiveness and monotonicity of the grid solution.

8.6.2 Classification of grid schemes

At the step of the grid approximation construction, the left-hand side of the transport equation (see Eq. (8.1)) can be written in two forms. In the first form it is suggested, that the term $\vec{\Omega}\cdot\vec{\nabla}\psi$ in Eq. (8.2) is the derivative in the direction $\vec{\Omega}$:

$$\vec{\Omega}\cdot\vec{\nabla}\psi = \frac{\partial\psi}{\partial\vec{\Omega}}\,.$$

Then the solution $\psi(\vec{r},\vec{\Omega})$ is defined by the formula

$$\begin{aligned}\psi(\vec{r},\vec{\Omega}) \;=\; & \overline{\psi}(\vec{r}^{\,*},\vec{\Omega})\,\exp\left(-\int_0^{|\vec{r}-\vec{r}^{\,*}|} K_{\rm ext}(\vec{r}^{\,*}+\xi\,\vec{\Omega})\,{\rm d}\xi\right)\\ & +\int_0^{|\vec{r}-\vec{r}^{\,*}|} B(\vec{r}^{\,*}+\xi\,\vec{\Omega},\vec{\Omega})\exp\left(-\int_\xi^{|\vec{r}-\vec{r}^{\,*}|} K_{\rm ext}(\vec{r}^{\,*}+\xi'\,\vec{\Omega})\,{\rm d}\xi'\right)\,{\rm d}\xi\,, \quad (8.18)\end{aligned}$$

If one considers the term $\vec{\Omega}\cdot\vec{\nabla}\psi$ as an inner product of two vectors in (x, y, z) geometry, the following expression for $\hat{L}$ can be written:

$$\hat{L}\psi = \gamma\frac{\partial\psi}{\partial z} + \eta\frac{\partial\psi}{\partial y} + \xi\frac{\partial\psi}{\partial x} + K_{\text{ext}}\,\psi\,. \tag{8.19}$$

The method of grid scheme construction based on Eq. (8.18) is known as the characteristics method (see Fig. 8.7) because integration in (8.18) is carried out either along the whole characteristics of the operator $\hat{L}$, defined by Eq. (8.1) (segment AB in Fig. 8.8) or along the characteristics segment, located inside a single mesh (segment A′B′ in Fig. 8.8). In the first case we obtain *long characteristics schemes* (section 8.7). In the second case we come to *short characteristics schemes* (section 8.8). Construction of *integro-interpolational schemes*

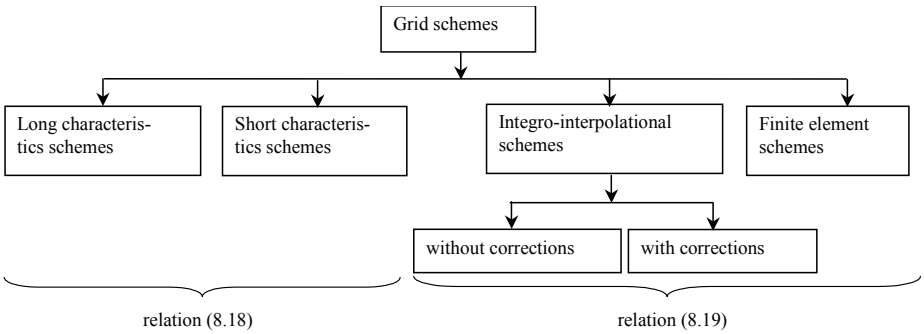

Fig. 8.7. Classification of schemes.

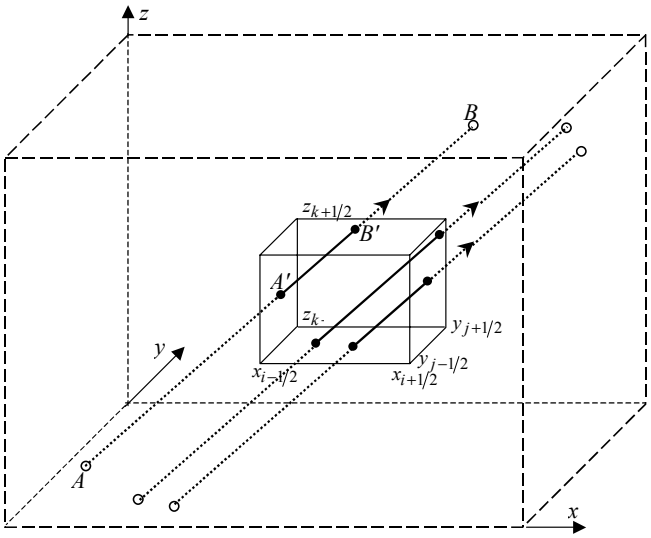

Fig. 8.8. Transfer of long characteristics through the whole calculation region (line AB) and one grid mesh (segment A′B′).

(section 8.9) (Samarsky, 1989) and *finite element schemes* (section 8.10) are based on Eq. (8.19). The grid scheme classification used in this chapter (that is close to widely accepted one), is depicted in Fig. 8.7.

Integro-interpolational schemes may be divided into schemes *with corrections* (section 8.9.2) and schemes without corrections (section 8.9.1). In the case of schemes with corrections, each mesh is calculated first according to a non-positive and non-monotonous scheme of a high order of accuracy. If the grid solution is negative or possesses non-physical oscillations, the mesh is recalculated via a lower-order accuracy scheme, which guarantees the solution positivity and, possibly, oscillation smoothing.

If scheme equations contain spatial moments of higher order (besides zero moments), the scheme is called *a nodal one* (section 8.9.3). Nodal schemes were developed for each class, presented in Fig. 8.7. It is suggested that such schemes may include grids with large meshes. Utilizing nodal schemes leads to an increase in the calculation scope, the calculation accuracy and the complexity being simultaneously increased. On the other hand nodal schemes provide accurate calculations with coarser grids compared to lower-order accuracy schemes. This feature leads to reduction of calculation time.

It is worth noting, that the characteristics schemes are often used in atmosphere optics problems (see section 8.7). Recently the code RADUGA-5.1(P) (Nikolaeva et al., 2005a,b), based on integro-interpolational schemes (section 8.9), has been successfully applied to the solution of the abovementioned problems (section 8.13.2).

8.7 Long characteristics schemes

Long characteristics schemes were initially developed for the case of one-dimensional spherical geometry (Vladimirov, 1958). They have since been extended to problems with Cartesian (x, y, z) geometry (Suslov, 1988; Postma and Viujic, 1999; Evans, 1998). Very informative monographs (Sushkevich et al., 1990; Sushkevich, 2005) contain, in particular, algorithms of long and short characteristics in Cartesian and spherical geometries.

The calculation starts with the introduction of a spatial grid and definition of a set of characteristics for Eq. (8.1) (see segment AB in Fig. 8.8, where all characteristics are depicted by arrows). Several characteristics pass in each direction $\vec{\Omega}$ can intersect a spatial mesh (see segment A′B′ in Fig. 8.8), where intersection points of characteristics and mesh edges are denoted by spots.

Using spatial moments of the function $B(\vec{r}, \vec{\Omega})$ in a mesh, we calculate the values of this function at each point of each characteristic inside the mesh. The values of the solution $\psi(\vec{r}, \vec{\Omega})$ at points of characteristics can be found using Eq. (8.18). To decrease the calculation time, the exponents in Eq. (8.18) can be replaced by fractional-polynomial approximations (so called Padé approximations) (Marchuk and Lebedev, 1981), which have the form $\exp(-h) \simeq (2-h)/(2+h)$ or the form $\exp(-h) \simeq 1/(1+h)$.

The zero spatial moment (8.15) of the solution in each mesh can be found as the average of the solution over all characteristics in the same direction $\vec{\Omega}$, intersecting the mesh (see Fig. 8.8). Obviously, the obtained grid solution generally does not satisfy the balance relation. For this the special normalizing coefficients must be introduced.

The long characteristics schemes are in some sense equivalent to the MC methods. Just like the MC schemes, they always generate positive solutions under positive sources. Besides, the schemes are capable of taking into account the whole region with inhomogeneities accurately. On the other hand, the characteristics method demands calculations for a large number of directions $\vec{\Omega}$ for those problems, where the MC method has to use many histories, and so the long characteristics method is a very time-consuming one.

8.8 Short characteristics schemes

In short characteristics schemes, the edges of each mesh are divided into 'entering' (through them radiation enters the mesh) and 'outgoing' (through them radiation leaves the mesh). For example in (x, y, z) geometry, if values γ and φ which define the transport direction $\vec{\Omega}$, belong to the octant $\{0 < \gamma < 1, 0 < \varphi < \pi/2\}$, then radiation enters the calculation region via the boundaries $x = x_{1/2}$, $y = y_{1/2}$ and $z = z_{1/2}$ (see Fig. 8.9). Therefore, 'entering' edges are $x = x_{i-1/2}$, $y = y_{j-1/2}$, $z = z_{k-1/2}$, and 'outgoing' ones are $x = x_{i+1/2}$, $y = y_{j+1/2}$, $z = z_{k+1/2}$ (see Fig. 8.9).

The grid scheme solution at 'entering' edges is approximated by some continuous functions. Further under these assumptions the transport equation solution is defined via Eq. (8.18) both inside the mesh and at its 'outgoing' edges. At last, the solution moments are calculated both inside the mesh and at the 'outgoing' edges.

According to the *SC (Step Characteristics) scheme* (Lathrop, 1969) the solution at each 'entering' edge is represented by a constant, which is equal to the corresponding value of the zero spatial moment (see Eq. (8.15)). Equations for the grid solution calculation can be written in the following form:

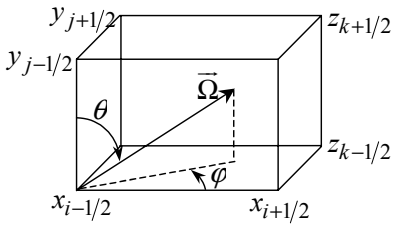

Fig. 8.9. Mesh in (x, y, z) geometry.

$$\begin{aligned}
\psi_{i+1/2,j,k} &= a_{x,x}\,\psi_{i-1/2,j,k} + a_{y,x}\,\psi_{i,j-1/2,k} + a_{z,x}\,\psi_{i,j,k-1/2} + a_{B,x}\,B_{i,j,k}\,,\\
\psi_{i,j+1/2,k} &= a_{x,y}\,\psi_{i-1/2,j,k} + a_{y,y}\,\psi_{i,j-1/2,k} + a_{z,y}\,\psi_{i,j,k-1/2} + a_{B,y}\,B_{i,j,k}\,,\\
\psi_{i,j,k+1/2} &= a_{x,z}\,\psi_{i-1/2,j,k} + a_{y,z}\,\psi_{i,j-1/2,k} + a_{z,z}\,\psi_{i,j,k-1/2} + a_{B,z}\,B_{i,j,k}\,,\\
\psi_{i,j,k} &= a_{x,0}\,\psi_{i-1/2,j,k} + a_{y,0}\,\psi_{i,j-1/2,k} + a_{z,0}\,\psi_{i,j,k-1/2} + a_{B,0}\,B_{i,j,k}\,.
\end{aligned} \tag{8.20}$$

where $B_{i,j,k}$ is the zero spatial moment of $B(x,y,z)$ in the mesh:

$$B_{i,j,k} = \frac{1}{\Delta x_i \Delta y_j \Delta z_k} \int_{x_{i-1/2}}^{x_{i+1/2}} \mathrm{d}x \int_{y_{j-1/2}}^{y_{j+1/2}} \mathrm{d}y \int_{z_{k-1/2}}^{z_{k+1/2}} \mathrm{d}z B(x,y,z)\,, \tag{8.21}$$

and coefficients $a_{t,h}$, $t = x,y,z,B$, $h = x,y,z,0$ depend on the transport direction $\vec{\Omega}\,\{\gamma,\varphi\}$, the mesh size Δx_i, Δy_j, Δz_k, and the extinction coefficient

$$K_{i,j,k} = K_{\mathrm{ext}}(x_i, y_j, z_k)\,. \tag{8.22}$$

Here it is assumed that all coefficients of the transport equation in each mesh are constant.

Equation (8.20) allows us to find the zero moment $\psi_{i,j,k}$ at the mesh and the moments $\psi_{i+1/2,j,k}$, $\psi_{i,j+1/2,k}$, $\psi_{i,j,k+1/2}$ at the 'outgoing' edges, if the zero moment $B_{i,j,k}$ and $\psi_{i-1/2,j,k}$, $\psi_{i,j-1/2,k}$, $\psi_{i,j,k-1/2}$ at the 'entering' edges are known.

Hence, for each fixed transport direction $\vec{\Omega}\ \{\gamma,\varphi\}$, the grid solution can be defined recursively. Let the values γ and φ belong to the octant $\{0 < \gamma < 1, 0 < \varphi < \pi/2\}$. Then the calculation begins from the mesh $[x_{1/2},\ x_{3/2}] \times [y_{1/2},\ y_{3/2}] \times [z_{1/2},\ z_{3/2}]$. The radiation intensity values at 'entering' edges, i.e. values $\psi_{1/2,1,1}$, $\psi_{1,1/2,1}$, $\psi_{1,1,1/2}$, are known from the boundary conditions (8.6). Eq. (8.20) permits us to find the values of the solution at 'outgoing' edges, i.e. the values $\psi_{3/2,1,1}$, $\psi_{1,3/2,1}$, $\psi_{1,1,3/2}$. They can be considered as moments at 'entering' edges for meshes $[x_{3/2},\ x_{5/2}]\times[y_{1/2},\ y_{3/2}]\times[z_{1/2},\ z_{3/2}]$, $[x_{1/2},\ x_{3/2}]\times[y_{3/2},\ y_{5/2}]\times[z_{1/2},\ z_{3/2}]$ and $[x_{1/2},\ x_{3/2}]\times[y_{1/2},\ y_{3/2}]\times[z_{3/2},\ z_{5/2}]$, correspondingly. So we can calculate all the grid solution values via sorting out successively all the meshes according to the increase of indices.

For each fixed transport direction $\vec{\Omega}$ different sequences of mesh calculations may be used. Two possible ways for mesh sorting out in a single z-layer are shown in Fig. 8.10. Note that the calculation sequence for $\vec{\Omega}$ directions is indifferent in the case of Cartesian spatial geometry.

We should also note that, according to formula (8.20), the solution moment at an 'outgoing' edge is the linear combination of right-side moments and solution moments at 'entering' edges. For example, the coefficient $a_{x,x}$ defines, what fraction of radiation, entering the mesh via the edge $x = x_{i-1/2}$, reaches the edge $x = x_{i+1/2}$.

Eq. (8.20) is illustrated in Fig. 8.11. All characteristics are depicted by arrows, and the shaded square $S_{x,x}$ corresponds to the share of edge $x = x_{i+1/2}$, illuminated by radiation, entering the mesh via the edge $x = x_{i-1/2}$. Square $S_{x,z}$ is a similar share of edge $z = z_{k+1/2}$.

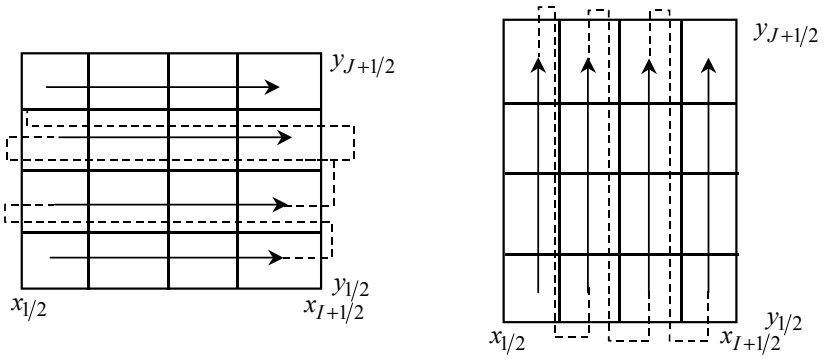

Fig. 8.10. Sequences of mesh calculation for the layer $(z_{k-1/2},\ z_{k+1/2})$.

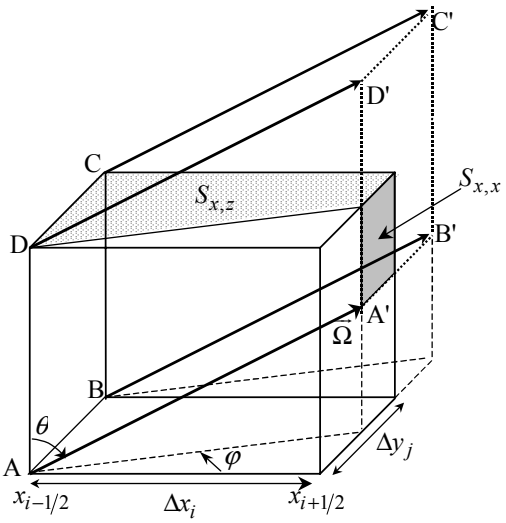

Fig. 8.11. Characteristics ($\nearrow$) of the transport equation in a mesh.

The corresponding to pair $x = x_{i+1/2}$ and $x = x_{i-1/2}$ coefficient $A_{x,x}$ of the exact solution $\psi^{exact}(x, y, z)$ can be defined by the equality

$$A_{x,x} = U/V\,,$$

where

$$\begin{aligned} U &= \frac{1}{S_{x,x}} \int_{S_{x,x}} \mathrm{d}y\,\mathrm{d}z\,\psi^{\mathrm{exact}}(x_{i+1/2}, y, z)\,, \\ V &= \frac{1}{\Delta y_j\,\Delta z_k} \int_{y_{j-1/2}}^{y_{j+1/2}} \mathrm{d}y \int_{z_{k-1/2}}^{z_{k+1/2}} \mathrm{d}z \psi^{\mathrm{exact}}(x_{i-1/2}, y, z)\,. \end{aligned}$$

Similarly, the remaining coefficients $A_{t,h}$ can be defined.

Some of coefficients $A_{t,h}$ are equal to zero. It means that radiation from the corresponding 'entering' edge does not reach the corresponding 'outgoing' edge. For example, if $tg\varphi < \Delta y_j/\Delta x_i$, then radiation from the edge $y = y_{j-1/2}$ does not reach the edge $y = y_{j+1/2}$ and $A_{y,y} = 0$ (see Fig. 8.11).

Assuming, that the exact solution $\psi^{\text{exact}}(x, y, z)$ is a constant at each mesh edge, we can define the coefficients of SC scheme as coefficients of the exact solution:

$$a_{t,h} = A_{t,h}|_{\psi^{\text{exact}}(x,y,z)=\text{const}} ,$$

see above. In particular, if the coefficient $A_{t,h} = 0$, then the corresponding coefficient of the SC scheme is also equal to zero.

The features of the SC scheme discussed above permit us to calculate both smooth solutions and discontinuous ones in a correct way. This is confirmed by the calculation practice as well. At the same time, the scheme is of first-order accuracy only (in the uniform norm) (Nikolaeva, 2004), i.e. the parameter q in the estimation (8.17) is equal to 1.

To increase the scheme accuracy, it is necessary to exploit more precise, possibly positive, approximations of the solution at 'entering' mesh edges. Constructing such approximations, we have to use solution moments of some adjacent meshes. The piecewise constant function (Mathews, 1999) and the exponent of linear function (Castriani and Adams, 1995) represent examples of positive approximations.

More accurate representations may be created in the frames of nodal schemes, where both zero moments and the ones of higher order are included. For example, using moments

$$\psi^{1,y}_{i+1/2,j,k} = \frac{3}{\Delta y_j\, \Delta z_k} \int_{y_{j-1/2}}^{y_{j+1/2}} \mathrm{d}y \bar{P}_1(y) \int_{z_{k-1/2}}^{z_{k+1/2}} \mathrm{d}z\, \psi(x_{i+1/2}, y, z)\,,$$

$$\psi^{1,z}_{i+1/2,j,k} = \frac{3}{\Delta y_j\, \Delta z_k} \int_{y_{j-1/2}}^{y_{j+1/2}} \mathrm{d}y \int_{z_{k-1/2}}^{z_{k+1/2}} \mathrm{d}z \bar{P}_1(z)\, \psi(x_{i+1/2}, y, z)\,,$$

compare with (8.16), we can construct the following linear approximation

$$\psi(x_{i+1/2}, y, z) \simeq \psi_{i+1/2,j,k} + \bar{P}_1(y)\, \psi^{1,y}_{i+1/2,j,k} + \bar{P}_1(z)\, \psi^{1,z}_{i+1/2,j,k}\,. \qquad (8.23)$$

The zero and the first moments of this expansion are equal to corresponding moments of the exact solution. Similarly, approximations with polynomials of higher order can be constructed.

As these approximations are not always positive, the corresponding grid schemes will not be positive as well (Azmy, 1992; Elsawi et al., 2003). The positive nodal scheme of short characteristics was successfully constructed based on long characteristics method applied to each spatial mesh (Santandrea and Sanchez, 2002).

It should be noted that all the considered schemes have no corrections.

8.9 Integro-interpolational schemes

8.9.1 Zero spatial moments schemes without corrections

The construction of integro-interpolational schemes in a mesh is always based on a *balance relation*, which can be obtained as a result of action of the integral operator

$$\frac{1}{\Delta x_i \Delta y_j \Delta z_k} \int_{x_{i-1/2}}^{x_{i+1/2}} \mathrm{d}x \int_{y_{j-1/2}}^{y_{j+1/2}} \mathrm{d}y \int_{z_{k-1/2}}^{z_{k+1/2}} \mathrm{d}z$$

on Eqs (8.1), (8.19). In (x, y, z) geometry, the balance relation has a form

$$\begin{aligned}(\psi_{i+1/2,j,k} - \psi_{i-1/2,j,k})\,\xi/\Delta x_i + (\psi_{i,j+1/2,k} - \psi_{i,j-1/2,k})\,\eta/\Delta y_j \\ +(\psi_{i,j,k+1/2} - \psi_{i,j,k-1/2})\,\gamma/\Delta z_k + K_{i,j,k}\,\psi_{i,j,k} = B_{i,j,k}\,. \qquad (8.24)\end{aligned}$$

Here values $\psi_{i,j,k}$, $\psi_{i\pm1/2,j,k}$, $\psi_{i,j\pm1/2,k}$, $\psi_{i,j,k\pm1/2}$, $B_{i,j,k}$, $\sigma_{t,i,j,k}$ are defined by the expressions (8.15), (8.21) and (8.22).

To uniquely determine values $\psi_{i,j,k}$, $\psi_{i+1/2,j,k}$, $\psi_{i,j+1/2,k}$, $\psi_{i,j,k+1/2}$, the values $\psi_{i-1/2,j,k}$, $\psi_{i,j-1/2,k}$, $\psi_{i,j,k-1/2}$, $B_{i,j,k}$ being known, we join the *additional equations* to the exact balance relation (8.24). The *WDD (Weighted Diamond Difference) scheme* is often used in calculations. The relations for radiation directions from the octant $\{0 < \gamma < 1,\ 0 < \varphi < \pi/2\}$, being written in the form

$$\begin{aligned}\psi_{i,j,k} &= (\psi_{i+1/2,j,k} + p_{x,i,j,k}\,\psi_{i-1/2,j,k})/(1 + p_{x,i,j,k})\,, \\ \psi_{i,j,k} &= (\psi_{i,j+1/2,k} + p_{y,i,j,k}\,\psi_{i,j-1/2,k})/(1 + p_{y,i,j,k})\,, \\ \psi_{i,j,k} &= (\psi_{i,j,k+1/2} + p_{z,i,j,k}\,\psi_{i,j,k-1/2})/(1 + p_{z,i,j,k})\,, \qquad (8.25)\end{aligned}$$

are used in WDD as additional equations. Here the weight parameters $p_{x,i,j,k}$, $p_{y,i,j,k}$, $p_{z,i,j,k}$ belong to the segment [0,1].

Traditionally, before solving the equations (8.24) and (8.25) in arbitrary mesh, the first moment $\psi_{i,j,k}$ is defined. After that the moments at 'outgoing' edges are calculated by means of Eqs (8.25). The approach permits to reduce the number of arithmetic operations. Further the sequential mesh sorting, which was outlined above for the SC scheme, is applied.

Features of a given WDD scheme depend on its weight parameters. Two WDD schemes are often used: the *DD (Diamond Difference) scheme* and the *St (Step) scheme*. Their weights are defined by the equalities $p_{x,i,j,k} = p_{y,i,j,k} = p_{z,i,j,k} = 1$ and $p_{x,i,j,k} = p_{y,i,j,k} = p_{z,i,j,k} = 0$, correspondingly. As has been shown (Madsen, 1975) only the DD scheme among all WDD schemes possesses second-order accuracy in mean square norm. The WDD schemes with other weights are of the first-order accuracy.

From the first glance, the obtained estimations indicate, that it is only worth using the DD scheme for transport problems. However, as calculation practice shows, really the DD solutions turn out to be negative or contain non-physical oscillations.

We would like to explain the reason for the mentioned effects. For this purpose, we explicitly rewrite the calculation formulas of DD scheme for cubic grid ($\Delta = \Delta x_i = \Delta y_j = \Delta z_k$). For the mesh with indices i, j, k we have the following expressions:

$$
\begin{aligned}
&\psi_{i,j,k} \\
&= \frac{\xi\,\psi_{i-1/2,j,k} + \eta\;\psi_{i,j-1/2,k} + \gamma\,\psi_{i,j,k-1/2} + \Delta\,B_{i,j,k}/2}{\gamma + \xi + \eta + K_{i,j,k}\,\Delta/2}\,, \\
&\psi_{i+1/2,j,k} \\
&= \frac{(\xi - \gamma - \eta - K_{i,j,k}\Delta/2)\,\psi_{i-1/2,j,k} + 2\eta\,\psi_{i,j-1/2,k} + 2\gamma\,\psi_{i,j,k-1/2} + \Delta\,B_{i,j,k}}{\gamma + \xi + \eta + K_{i,j,k}\,\Delta/2}\,, \\
&\psi_{i,j+1/2,k} \\
&= \frac{2\xi\,\psi_{i-1/2,j,k} + (\eta - \gamma - \xi - K_{i,j,k}\Delta/2)\;\psi_{i,j-1/2,k} + 2\gamma\,\psi_{i,j,k-1/2} + \Delta\,B_{i,j,k}}{\gamma + \xi + \eta + K_{i,j,k}\,\Delta/2}\,, \\
&\psi_{i,j,k+1/2} \\
&= \frac{2\xi\,\psi_{i-1/2,j,k} + 2\eta\,\psi_{i,j-1/2,k} + (\gamma - \xi - \eta - K_{i,j,k}\Delta/2)\,\psi_{i,j,k-1/2} + \Delta\,B_{i,j,k}}{\gamma + \xi + \eta + K_{i,j,k}\,\Delta/2}\,.
\end{aligned}
\tag{8.26}
$$

As one can verify, these equations are satisfied identically in the case of the linear solution

$$\psi(x, y, z) = A + B\,x + C\,y + D\,z\,,$$

where A, B, C, D are arbitrary constants. It confirms the fact, that DD scheme is of second-order accuracy for smooth solutions. In the addition, zero solution moment $\psi_{i,j,k}$ is always positive for positive $B_{i,j,k}$ and moments on 'entering' edges. Nevertheless, moments on 'outgoing' edges may be negative, if $\left|\psi_{i-1/2,j,k} - \psi_{i,j-1/2,k}\right| \gg 1$ or $\left|\psi_{i-1/2,j,k} - \psi_{i,j,k-1/2}\right| \gg 1$ or $\left|\psi_{i,j-1/2,k} - \psi_{i,j-1/2,k}\right| \gg 1$, i.e. if the grid solution decreases too quickly (see Fig. 8.12).

Let $\psi_{i,j-1/2,k} = \psi_{i,j,k-1/2} = \psi_{i+1,j-1/2,k} = \psi_{i+1,j,k-1/2} = B_{i,j,k} = 0$. Then Eq. (8.26) can be written in form

$$\psi_{i+1/2,j,k} = \rho\,\psi_{i-1/2,j,k}\,,\;\; \psi_{i+3/2,j,k} = \rho^2\,\psi_{i-1/2,j,k}\,,\;\; \rho = \frac{\xi - \gamma - \eta - K_{i,j,k}\Delta/2}{\gamma + \xi + \eta + K_{i,j,k}\Delta/2}\,.$$

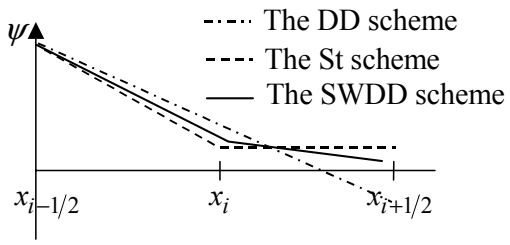

Fig. 8.12. WDD schemes solution in a mesh.

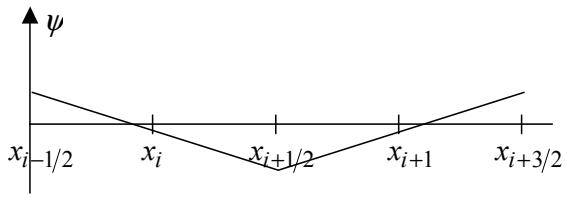

Fig. 8.13. DD scheme solution for a pair of meshes.

As $\xi - \gamma - \eta - \sigma_{t,i,j,k}\Delta/2 < 0$, the coefficient ρ is negative and non-physical oscillations in DD solutions arise (see Fig. 8.13).

Therefore, the additional relations in the DD scheme are too coarse to calculate quickly varying functions.

Calculation formulas of the St scheme with a cubic mesh can be written in the form

$$\begin{aligned}\psi_{i+1/2,j,k} &= \psi_{i,j,k+1/2} = \psi_{i,j,k+1/2} = \psi_{i,j,k} \\ &= \frac{\xi\,\psi_{i-1/2,j,k} + \eta\,\psi_{i,j-1/2,k} + \gamma\psi_{i,j,k-1/2} + \Delta B_{i,j,k}}{\gamma + \xi + \eta + K_{i,j,k}\Delta}\,.\end{aligned}$$

These equations are converted into identities only if the solution is constant. It is the consequence of the fact, that St scheme is of first-order accuracy for smooth solutions. Thus, although this scheme is positive (see Fig. 8.12) it is of low accuracy.

So we have a non-positive and non-monotonic DD scheme of second-order accuracy and a positive and monotonic St scheme of first-order accuracy. This fact confirms the known theorem by S. K. Godunov: *it is impossible to construct monotonic linear discretizations for hyperbolic systems of equations that would be of second- or of higher-order accuracy, if one is restricted by zero solution moments only.*

For this reason schemes of two different classes have been developed. They are

- positive and monotonic schemes of a higher-order accuracy as compared to the St scheme,
- non-positive and non-monotonic schemes, which more rarely generate negative and non-physical oscillatory grid solutions for practical problems as compared to the DD scheme.

The first class includes WDD schemes with a more flexible algorithm with respect to the definition of weights. One such algorithm leads to the *SWDD (Special WDD) scheme* (Bass and Nikolaeva, 1997; Nikolaeva, 2004), its weights are calculated using the following equations:

$$a_{x,x}(p_x, p_y, p_z) = \bar{a}_{x,x}\,, \quad a_{y,y}(p_x, p_y, p_z) = \bar{a}_{y,y}\,, \quad a_{z,z}(p_x, p_y, p_z) = \bar{a}_{z,z}\,.$$

Here the values $a_{x,x}, a_{y,y}, a_{z,z}$ and $\bar{a}_{x,x}, \bar{a}_{y,y}, \bar{a}_{z,z}$ are coefficients of Eq. (8.20) for the SWDD scheme and for the SC scheme respectively. As it turned out, the following assertions are valid:

- All coefficients of the SWDD scheme are non-negative.
- Each non-diagonal coefficient ($a_{t,h}$ for $t \neq h$) of the SWDD scheme is close to the corresponding coefficient of SC scheme, if the spatial grid is a sufficiently fine one.
- If any coefficient of the SC scheme is equal to zero, then the corresponding coefficient of the SWDD scheme is equal to zero as well.

In other words, the features of integro-interpolational SWDD scheme are similar to those of the SC scheme of short characteristics, and so the SWDD scheme also can be used for calculation of discontinuous solutions (Nikolaeva, 2004). It should be noted, however, that the SWDD scheme is slightly more accurate than the SC one. In addition, the SWDD scheme, being convenient for the implementation (the code RADUGA-5.1(P), see section 8.13.2), has demonstrated its advantages in atmospheric optics and radiation protection problems.

It should mentioned, that the SWDD scheme weights in any mesh depend on the radiation transport direction $\vec{\Omega}$ (that is, on γ and φ, mesh sizes Δx_i, Δy_j, Δz_k, and on the value of the extinction coefficient in the mesh $K_{i,j,k} = K_{\text{ext}}(x_i, y_j, z_k)$). Remember, that the grid solution inside a mesh is a positive piecewise linear function, see Fig. 8.12, whereas DD solution is a linear function, which can be negative (see Fig. 8.12).

The *MDSN*$_1$ *scheme* (Nikolaeva, 2004) is positive and monotonous one as well. Coefficients of the MDSN$_1$ scheme converge to coefficients of the SWDD scheme under grid condensing. But insofar as the grid is coarse, these two schemes are different.

Improved additional relations as compared to the DD scheme are used in schemes of the second class. Sometimes the additional relations include moments of adjacent meshes (Morel and Larsen, 1990; Adams, 1991). In other cases the relations are obtained with the help of the analytical solution of the transport equation (8.1), averaged over all spatial variables except some single variables (Azmy, 1988a; Zhougsheng et al., 1994). The *EC (Exponential) scheme* with non-linear additional relations (Barbucci and Pasquantonio, 1977) is worthly of special mention. It is the scheme with relations of the kind

$$\psi_{i,j,k} = \sqrt{\psi_{i+1/2,j,k}\ \psi_{i-1/2,j,k}} = \sqrt{\psi_{i,j+1/2,k}\ \psi_{i,j-1/2,k}} = \sqrt{\psi_{i,j,k+1/2}\ \psi_{i,j,k-1/2}}\,.$$

Schemes based on the quasi-stationary derivatives principle (Suslov and Pevey, 1997) are also of special interest. Differentiating the transport equation (8.1) with respect to each spatial variable and equating all second derivatives to zero (here the solution is suggested to be slowly varying), one can find approximate expressions for the first derivatives of $B(\vec{r}, \vec{\Omega})$. Using these expressions, more accurate representations for both $B(\vec{r}, \vec{\Omega})$ and the solution can be constructed.

8.9.2 Zero spatial moment schemes with corrections

The impossibility of constructing a positive and monotonous scheme of second-order accuracy forces us to use schemes with corrections. As a result *WDD schemes with corrections* have been actively developed. In these schemes, first a mesh is calculated via a DD scheme and then, if the grid solution turnes out to be a negative one or even oscillatory, the mesh is recalculated via a WDD scheme of first-order accuracy.

The earliest of the schemes is the *DD/St scheme*, where the mesh recalculation is carried out via the St scheme, if at least one of 'outgoing' edges provided a negative moment of the solution. However, correction of this kind is too rough, because the weight values undergo jumps inside a mesh. Thus, these schemes are positive, but non-monotonous ones.

More flexible corrections are exploited in the positive and non-monotonous *θ WDD scheme* (Rhoades and Engle, 1977; Petrovic and Haghighat, 1996). Finally, an algorithm of oscillation smoothing is included in the grid equations of the *AWDD (Adaptive WDD) scheme* (Carlson, 1976; Voloschenko and Germogenova, 1994). Here the user can choose the degree of oscillation smoothing via the specification of the parameter for monotonization of the solution. In *MDSN scheme* corrections the numerical algorithm relies on the condition of monotonicity of the grid solution (Voloschenko, 1981).

In multidimensional problems, both MDSN and AWDD schemes require the iterative construction of scheme equations in each mesh to ensure grid solution monotonocity for all variables. Usually one needs to use one or two iterations. Under many iterations, MDSN equations tend to equations of the monotonous $MDSN_1$ *scheme* (Nikolaeva, 2004). In slab geometry MDSN and MDSN1 schemes are equivalent.

Finally, in some cases corrections are carried out via an *MDSN scheme* in selected meshes, adjoint to the surfaces, where transport equation coefficients undergo discontinuities. Here it is presupposed that oscillations arise mainly in such meshes. Corrections are performed just in the mesh set. Numerical results show that monotonization techniques only slightly smooth oscillations.

8.9.3 Nodal schemes

To complete our review of modern numerical schemes for the solution of the transport equation, we describe the so-called the nodal integro-interpolational schemes. Spatial moments of zero- and first-order (and sometimes higher orders) are used in these schemes for the construction of grid equations.

Several balance relations are used in the scheme construction. Each of the balance relations is obtained via integration of the transport equation (8.1) over a spatial mesh with an appropriate weight function. In some nodal schemes, the additional relations are based on the non-positive polynomial (Walters, 1982, 1986; Badruzzaman, 1985; Azmy, 1988b; Warin, 1996; Voloschenko, 1997; Zmijarevic, 1999; Takeda and Yamamoto, 2001), the piecewise polynomial (Voronkov and Sychugova, 1997) or the exponential (Ullo et al., 1982) representations of a

grid solution in a mesh. Although these schemes have a high order of accuracy (up to four), usually they are neither positive nor monotonous.

Positive nodal integro-interpolational schemes are of lower-order accuracy (second to third) than non-positive ones. They are based on the approximation of the solution via piecewise constant (Mathews and Minor, 1991), piecewise linear (Mathews and Minor, 1993) or exponential linear (Walters et al., 1995; Wareing, 1997) functions.

Nodal schemes with corrections are also actively developed. They combine the preliminary grid calculation via non-positive and non-monotonous scheme of high order and its consequent recalculation via a positive and a partially monotonous scheme of a lower-order accuracy (Voloschenko, 1997; Shwetsov, 1997).

8.10 Finite element schemes

At preliminary step of the construction of finite elements schemes, a specific basis of functions $\{u_g(\vec{r},\vec{\Omega})\}$, $g = 1,\ldots,G$ is chosen. The solution in each mesh is represented by a linear combination:

$$\psi(\vec{r},\vec{\Omega}) \simeq \tilde{\psi}(\vec{r},\vec{\Omega}) = \sum_{g=1}^{G} u_g(\vec{r},\vec{\Omega})\, T_g\,.$$

Coefficients T_g are defined by equating mesh solution moments at mesh edges to corresponding moments of $\tilde{\psi}(\vec{r},\vec{\Omega})$ representation. Further the residual $R(\vec{r},\vec{\Omega})$ for the function $\tilde{\psi}(\vec{r},\vec{\Omega})$ via Eq. (8.1) is calculated:

$$R(\vec{r},\vec{\Omega}) = \hat{L}\tilde{\psi}(\vec{r},\vec{\Omega}) - B(\vec{r},\vec{\Omega})\,.$$

After that the scheme equations are defined via the integration of the equality $R(\vec{r},\vec{\Omega}) = 0$ over the mesh. Also some weight functions, which in the general case do not coincide with basis functions $u_g(\vec{r},\vec{\Omega})$, are used. The chosen functions $u_g(\vec{r},\vec{\Omega})$, defining grid solution form, are named finite elements.

Using only zero spatial moments and bilinear combinations of functions $u_g(\vec{r},\vec{\Omega})$, one can successfully construct an effective calculation scheme (Morel et al., 1993).

Using moments of high orders, nodal schemes of finite elements can be created (Hennart and del Valle, 1997; del Valle and Alonso, 2001).

8.11 The solution of the grid equation

The previous sections were aimed at the construction of the grid equation, approximating both the differential operator $\widehat{L}$ and the integral operator $\widehat{S}$ in the transport equation (8.1). As a result we find a system of linear algebraic equations

$$\widehat{L}^{\mathrm{grid}}\vec{\psi} = \widehat{S}^{\mathrm{grid}}\,\vec{\psi} + \vec{Q}\,, \tag{8.27}$$

where the vector $\vec{\psi}$ is formed by grid solution values in all meshes of spatially-angular grid, and grid operators $\widehat{L}^{\mathrm{grid}}$ and $\widehat{S}^{\mathrm{grid}}$ correspond to the differential operator $\widehat{L}$ and the integral operator $\widehat{S}$. In section 8.7 an explicit method, based on operator $\widehat{L}^{\mathrm{grid}}$ inversion, was presented. The system (8.27) is solved using the *simple iteration method*:

$$\vec{\psi}^{it+1} = (\widehat{L}^{\mathrm{grid}})^{-1}[\widehat{S}^{\mathrm{grid}}\,\vec{\psi}^{it} + \vec{Q}]\,. \tag{8.28}$$

Iterations are stopped when the relative variation of a scalar flux (i.e. solution averaged over angle variables) inside all spatial meshes is less then a value of ε (ε being specified by a user). Usually the values ε inside the interval (0.0001–0.001) are used in calculations.

Insofar as the operator $\widehat{S}^{\mathrm{grid}}$ describes light scattering processes, each new iteration adds to a grid solution contribution, provided photons undergo the next order of scattering. Therefore, the method (8.28) is known as *successive-orders-of-scattering method (SOSM)*.

If the size of the calculation region, measured in optical lengths, is large and absorption is weak (the typical situation for atmospheric optic problems in the visible and UV range), then on the average a photon undergoes a great number of scatterings, and so the iterative process (8.28) converges very slowly.

The Seidel scheme of Eq. (8.27) solving has proved to be more effective. It consists in obtaining solution values inside a separate octant at each iteration and subsequently utilizing them for Eq. (8.27) right-hand side calculation for other octants at the same iteration. This method is slightly more effective in solving Eq. (8.27) as compared to SOSM. Two-layer iterative schemes have proved to be even more effective. Their equations can be written in the form:

$$\widehat{L}^{\mathrm{grid}}\vec{\psi}^{it+1/2} = \widehat{S}^{\mathrm{grid}}\,\vec{\psi}^{it} + \vec{Q}\,, \quad \vec{\psi}^{it+1} = \vec{\psi}^{it+1/2} + \vec{\delta}^{it+1/2} \tag{8.29}$$

The equations for corrections $\vec{\delta}^{it+1/2}$ are constructed based on the fact that the equation for a grid solution error $\vec{E}^{it+1/2} = \vec{\psi} - \vec{\psi}^{it+1/2}$ satisfies the following relation:

$$\widehat{L}^{\mathrm{grid}}\vec{E}^{it+1/2} = \widehat{S}^{\mathrm{grid}}\,\vec{E}^{it+1/2} + \widehat{S}^{grid}(\vec{\psi}^{it} - \vec{\psi}^{it+1/2})\,.$$

Hence, the correction $\vec{\delta}^{it+1/2}$ can be naturally defined via some approximations of the vector $\vec{E}^{it+1/2}$. In a wide class of methods, a correction $\vec{\delta}^{it+1/2}$ can be sought *in the low approximation over angular variables* (Adams and Larsen, 2002), vector $\vec{\delta}^{it+1/2}$ being a linear function or a constant in each octant with respect to angular variables. Similar methods were successfully exploited in radiation shielding problems, because they make it possible to decrease the number of iterations tens or hundreds of times. But they are proved to be inapplicable in atmospheric optics problems, where light is scattered mostly in the forward direction and the correction $\vec{\delta}^{it+1/2}$ cannot be approximated by a polynomial of a low order. For this case, *multigrid angular methods* were developed, where calculations are performed at a sequence of angular grids for each iteration (Morel and Manteuffel, 1991; Pautz and Morel, 1999). Correction to a finer grid so-

lution is obtained via a coarser grid calculation. After adding all the obtained corrections, a new iteration begins with the finest grid.

All listed methods are effective (the number of iterations decreases in order), if only the correction equations are *consistent with* initial grid (Eq. (8.27)), i.e. if correction equations are a consequence of Eq. (8.27). It should be noted that the consistent correction system is more complicated as compared to the inconsistent one.

An effective iterative scheme construction for problem (8.27) is rather difficult due to the fact that the operator $(\widehat{L}^{\text{grid}})^{-1}\widehat{S}^{\text{grid}}$ is not self-adjoint in practical problems. Among all methods developed for systems of type (8.27), only the methods by Krylov (Morel, 2005), which do not use the suggestion of the operator self-adjointness, are proved to be applicable here. In these methods, the corrections $\vec{\delta}^{it+1/2}$ can be presented by the linear combination of vectors $\vec{v}_\mu$:

$$\vec{\delta}^{it+1/2} = \sum_{\mu=1}^{\mathcal{M}} \vec{v}_\mu \, \beta_\mu \, .$$

The vectors $\vec{v}_\mu$ should be chosen from the space formed by residual vectors

$$\{\vec{r}_\mu, \mu = 1, \ldots, M\} \colon \vec{r}_1 = (\widehat{L}^{\text{grid}} - \widehat{S}^{\text{grid}})\vec{\psi}^{it+1/2} - \vec{Q} \, , \quad \vec{r}_\mu = (\widehat{L}^{\text{grid}} - \widehat{S}^{grid}) \, \vec{r}_{\mu-1} \, .$$

The coefficients β_μ can be found from the condition of the residual minimum for equations (8.27) in mean square norm, i.e. from the minimum condition for the sum of squares of elements of the vector

$$\vec{Y} = (\widehat{L}^{\text{grid}} - \widehat{S}^{\text{grid}}) \, (\vec{\psi}^{it+1/2} + \sum_{\mu=1}^{\mathcal{M}} \vec{v}_\mu \, \beta_\mu) - \vec{Q} \, .$$

As a result, coefficients β_μ are defined by a system of linear algebraic equations of the order $\mathcal{M} \times \mathcal{M}$.

In each version of the methods by Krylov the vectors $\vec{v}_\mu$ are constructed in own manner, based on vectors $\vec{r}_\mu$. The conjugate gradient method, the least squares technique, the quasi-minimal residual algorithm, the generalized minimal residual method and many other approaches use different ways to construct and also to store vectors $\vec{v}_\mu$. The number $\mathcal{M}$ of vectors is also different in different approaches.

The acceleration degree of methods by Krylov is increased when the number $\mathcal{M}$ of vectors $\vec{v}_\mu$ increases, but the calculation of vectors and scalar products is very time-consuming. If the number $\mathcal{M}$ is too large, the method is not effective.

8.12 Technique of transport equation solving by the parallel discrete ordinates method

The appearance of parallel-architecture computers has led to a new step in the development of numerical techniques. Obviously, the parallel algorithm construction should correspond to architecture particularities of concrete multiprocessor computers.

There are two main types of multiprocessor systems. In *weakly connected systems with distributed memory* each processor possesses its own disk and operative memory and is able to send data to other processors only via a common network. The information exchange speed between different processors here is lower than one between a single processor and its operative memory. Such kinds of multiprocessor systems can contain a lot of processors (more than a thousand).

In *strongly connected systems* all the processors have an extensive *shared (common) memory*. By means of the shared memory the processors perform the information exchange. The operation system should be capable of preventing errors, which may arise when two or more processors simultaneously deal with the same memory cell. The number of processors in the strongly connected systems is essentially smaller than in weakly connected ones.

The modern architecture is the so-called nested parallelism, where a distributed-memory machine (called a *cluster*) has embedded nodes with several (2, 4, 8) processors. In these machines two mechanisms are used for the communication: (a) shared memory when processors belong to the same node; (b) network communication when the processors belong to the different nodes.

The *effectiveness* of a parallel algorithm is defined by the formula

$$\mathrm{Eff}(\mathcal{N}) = T(1)/[\mathcal{N}\,T(\mathcal{N})]100\%\,, \tag{8.30}$$

where $\mathcal{N}$ is processor number, T(1) is the calculation time for a single processor, $T(\mathcal{N})$ is the calculation time for $\mathcal{N}$ processors. Obviously, the more uniform is the calculation distribution among all the processors the higher is parallel algorithm effectiveness, and so the less time it takes for a single processor to exchange information with other processors.

The parallelizing technique depends on the problem type. If the line-by-line calculation is carried out, then a high effectiveness of parallelizing can be achieved by means of the uniform distribution of problems for different wavelengths among all processors.

A parallel algorithm for the long characteristics method can be reduced to the proportional distribution of the calculation of different characteristics among the processors (Dahmani et al., 2003).

The parallel algorithm for solving transport problems for a single wavelength can be based on the calculation region decomposition. In the case of the angular decomposition (Azmy, 1988b) at one iteration all nodes of angular quadrature are distributed among different processors and the solution at each node is calculated by the corresponding processor. This kind of parallelizing implies that each single processor should transmit to previously chosen summarizing processor solution values at all the meshes to provide the consequent scattering integral calculation. After that each processor should get from the summarizing processor the scattering integral values at all spatial meshes. Similar algorithms should be realized on strongly connected computers in order to increase the high calculation effectiveness under a great number of information exchange operations.

If a spatial decomposition is used, the calculation region is divided into subregions, incoming radiation fluxes being supposed to be known at the sub-region

boundary. The fluxes are known either from boundary conditions or via neighboring sub-region calculations at a previous iteration (Hanebutte and Lewis, 1991; Haghighat and Azmy, 1991; Baker et al., 1995; Pautz, 2001).

In some cases the decomposition is realized both on spatial and on angular variables (Dorr and Salo, 1995; Sjoden and Haghighat, 1997; Nowak and Nemanic, 1999; Fischer and Azmy, 2003). Specially developed expert systems permit the estimation of time and memory expenses for each decomposition type (spatial, angular or spatially-angular) for each concrete calculation (Patchimpattapong and Haghighat, 2003).

Different calculation procedures for sub-regions are possible. For example, each sub-region can be computed by own processor at each iteration (Haghighat and Azmy, 1991). In the last case the algorithm includes two iterative processes: one for the calculation of the scattering integral and yet another one for the calculation of the solution values at sub-region boundaries. Naturally, with the number of sub-regions the necessary number of iterations increases as well. Besides, the obtained grid solution usually does not coincide with that obtained by a single processor at each iteration. Special parallel acceleration algorithms should be developed in such cases.

Accordingly to the 'red-black algorithm' (Hanebutte and Lewis, 1991; Sjoden and Haghighat, 1997), all the sub-regions are specified as 'red' or 'black'. At each iteration either only 'red' sub-regions or only 'black' ones participate in the calculation procedure (see Fig. 8.14). It permits to obtain more accurate values of entering fluxes at sub-region boundaries at each iteration.

According to the 'diagonal scheme' (Baker et al., 1995; Dorr and Salo, 1995), for any transport direction $\vec{\Omega}$, a special sequence of sub-region calculations, based on chosen angular quadrature, is used. For example, calculation begins with the left lower corner for a direction $\vec{\Omega}\{\gamma, \varphi\}$ at $\{0 < \gamma < 1, 0 < \varphi < \pi/2\}$ (see Fig. 8.1). The sequence is shown in Fig. 8.15. A number, marking each sub-region in Fig. 8.15, denotes the iteration number of sub-region participation in the common calculation procedure. In this case the solution, obtained by the parallel method, coincides with one obtained via a single processor method. Thus, it makes possible to use, in a parallel calculation, procedure acceleration algorithms which have been developed for single-processor calculations.

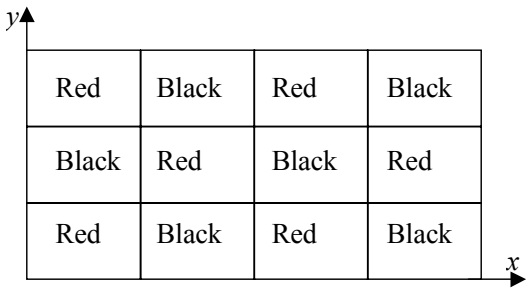

Fig. 8.14. Red-black algorithm scheme.

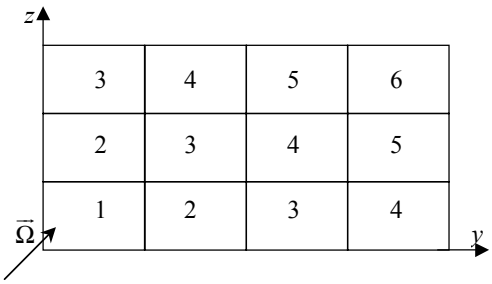

Fig. 8.15. Diagonal scheme.

8.13 Discrete ordinates codes

The project I3RC (http://i3rc.gsfc.nasa.gov) is of a great importance in 3D radiation transport (RT) codes verification. 'The goal of I3RC is to promote the improvement of algorithms that are used for all kinds of 3D RT processes in cloudy atmospheres. Activities include not only comparisons of results from state-of-the-art 3D RT codes, but also development of fast approximations that are more suitable for climate applications and community "open source" codes that distill the best current knowledge on how to treat the various interactions of ultraviolet, visible, and infrared photons with atmospheric constituents' (Cahalan et al., 2005).

For these purposes a number of test problems have been formulated for the verification of DOM and Monte Carlo algorithms. Participants in this project just created the codes providing calculation of the test problem with the required accuracy.

The main DOM code is SHDOM (Evans, 1998); recently RADUGAP-5.1(P) was included in the list of codes being used. Other results were obtained by Monte Carlo codes.

Now the project consists of three phases aimed at calculations of 1D, 2D and 3D problems accordingly. The authors suggest that 'the cloud and climate modeling community is further ahead of its remote sensing counterpart in incorporating the advances of 3D RT into its representation of radiative processes'.

8.13.1 SHDOM code

Currently the code SHDOM (Evans, 1998), belongs to widely used codes for the calculation of radiation transport in the terrestrial atmosphere (http://nit.colorado.edu/∼evans/shdom.html). Let us list its main attributes.

- The transport equation is solved in regions with Cartesian 1D, 2D and 3D coordinates (see Fig. 8.2).
- The radiation source is the Sun or thermal sources.
- Phase functions are represented by expansions on Legendre polynomials, the expansion order being arbitrary. To decrease the number of polynomials in the expansion, the delta-M method can be used (Wiscombe, 1977).

- Transport equation coefficients (the extinction coefficient, the single scattering albedo, the number of moments in phase function expansions) are defined by their values at spatial grid nodes.
- The boundary condition on the region external boundaries can be specified as periodicity condition or as boundary reflection law (in particular, the mirror reflection law and the Lambert reflection law are included).
- The transport equation for scattered radiation intensity is solved by the long characteristic method. Non-scattered radiation intensity is determined analytically.
- The spatial grid is defined by a user; it can be refined during the calculation procedure, if it is necessary for more accurate solution presentation.
- The simple iterative method with respect to scattering orders is used for solving grid equations; the iteration acceleration method, representing a version of the minimal residual method for a single-processor computer, is included.

The SHDOM is the numerical code for wide-range applications. Although a version of the long characteristics method is used in the code, it does not include the balance equation for a grid mesh. Besides, the acceleration method stability proof is absent. In some cases the iterative process does not converge.

8.13.2 The code RADUGA-5.1(P)

The code RADUGA-5.1(P) solves the transport equation in 2D and 3D regions under sufficiently common suggestions on source, phase functions and boundary conditions (Nikolaeva et al., 2005a,b). In particular, it may be used in such areas as atmospheric optics, radiation shielding problems, biomedicine, ray therapy, etc.

Below we outline the main characteristics of the RADUGA-5.1(P) code.

- The transport equation is solved in regions with Cartesian (x, y, z), (x, y) and cylindrical (r, ϑ, z), (r, ϑ), (r, z) coordinates (see Fig. 8.2 and Fig. 8.16).

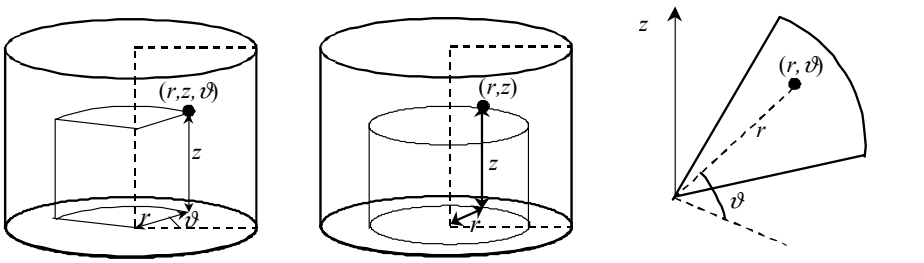

Fig. 8.16. Calculation regions with cylindrical coordinates.

- The radiation source may be given in the form of plane-parallel radiation flux (the Sun) or uniform radiation distribution in all directions (e.g., heated body).[1]
- Phase functions can be represented by expansions on Legendre polynomials, the expansion order being arbitrary, or by discrete-angular forms.
- Medium inhomogeneities are defined via surfaces of some model bodies (parallelepipeds, cylinders, spheres, cones, prisms and others). Transport equation coefficients (the extinction cross-section and the single scattering albedo) can be also defined at the nodes of a spatial grid.
- Periodic boundary conditions, the mirror reflection or the Lambert reflection law may be defined over any external boundary. The boundary condition at semi-infinity is also included.
- Angular quadratures of several widely used types (in particular, Carlson and Gauss quadratures) can be used for the scattering integral approximation; regular spatial grids are also used.
- Unscattered radiation intensity is calculated analytically. Grid schemes of first and second accuracy order of well known WDD family (DD, St, DD/St, AWDD, SWDD) are used for scattered radiation calculation.
- After spatial decomposition of a calculation region into sub-regions, the local spatial and angular grids may be introduced in each of them.
- Condensing of angular grids inside some solid angles is admissible.
- The simple iteration method with acceleration by the minimal residuals method is used for grid equations solving.
- The parallel algorithm is designed based on the international MPI standard. The spatial decomposition is used, each sub-region being calculated at each iteration.
- Calculation time is decreased while processor number $\mathcal{N}$ is increased, but the calculation time is not proportional to $\mathcal{N}$. So, the effectiveness of parallelizing is decreased as processor number increases (see (8.30)). In the case of a weakly connected computers with 20 processors the effectiveness is equal to 90%. If the number of processors is between 20 and 80, the effectiveness is near 65%. When the processor number is increased up to 200, the effectiveness is decreased up to 50%. The effectiveness reduction could be associated with increasing time of information exchange between processors.
- The code construction makes it possible to carry out calculations on weakly connected, on strongly connected and on clusters of multiprocessor computers, including personal computers.

Let us briefly outline the semi-infinity boundary condition, which is used in the case of a semi-infinite medium. An example is shown in Fig. 8.17, where both aerosol and cloud media are homogeneous and they possess a common vertical boundary.

[1] The code RADUGA-5.1(P) may be applied to solve problems with other sources. They are point isotropic, point anisotropic (in particular, source radiating in a cone of a small aperture) and ray sources.

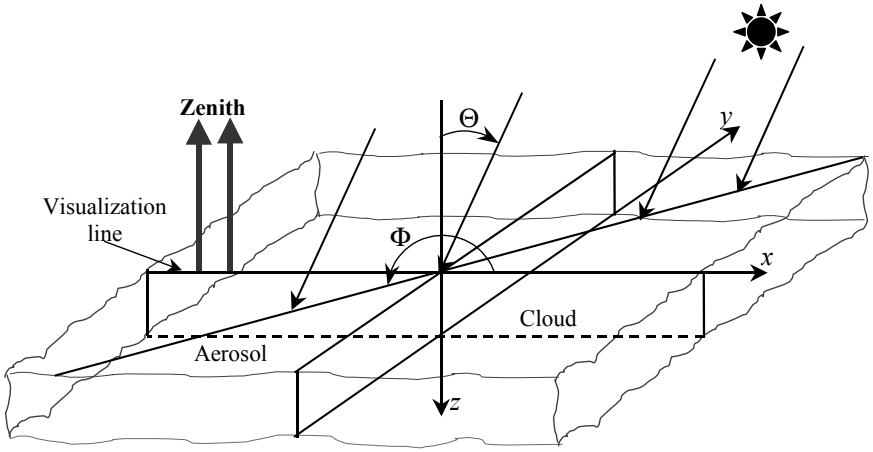

Fig. 8.17. Model problem calculation region.

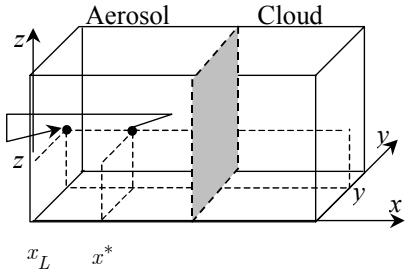

Fig. 8.18. Semi-infinity condition at the left boundary.

The semi-infinity condition with respect to variable x at the left boundary $x = x_L$ can be expressed by the formula (see Fig. 8.18):

$$\psi(x_L, y, z, \vec{\Omega}) = \psi(x^*, y, z, \vec{\Omega}), \quad -1 < \gamma < 1,\ 0 < \varphi < \pi/2 \quad \text{or } 3\pi/2 < \varphi < 2\pi, \tag{8.31}$$

Equation (8.31) guarantees the solution independence on the variable x far from the boundary of the media. Moreover, far from the boundary the solution can be approached by the constant, which can be defined from the corresponding 1D model.

Verification of the code RADUGA-5.1(P) was carried out, based on the model problem, depicted in Fig. 8.17. Aerosol scattering was modeled by the Heney–Greenstein phase function with asymmetry parameter $g = \omega_1/3 = 0.7$. The cloud C1 phase function (Kokhanovsky, 2006) was obtained based on Mie theory for the wavelength 412 nm. The asymmetry parameter g is equal to 0.86. Layer height is equal to 4 km, cloud optical thickness is chosen to be 30, aerosol optical thickness is equal to 1.2. Photons enter the layer only via the top boundary $z = 0$ (see Fig. 8.17).

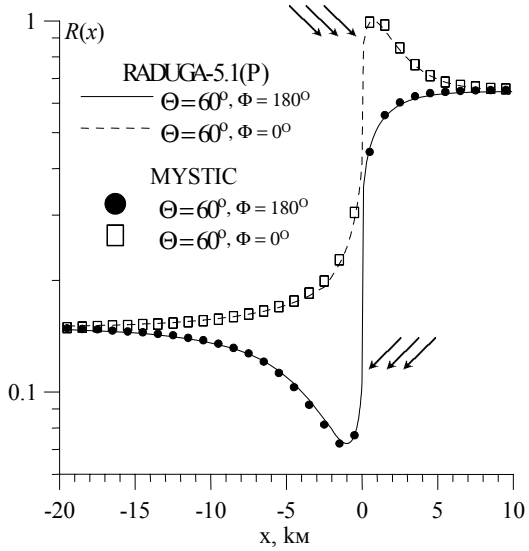

Fig. 8.19. Brightness coefficient in the model problem.

The brightness coefficients $R(x) = \pi\,\psi(x, 0, 0)/(F_0 \cos\Theta)$ for the radiation reflected in the zenith at the visualization line for two solar light directions $\Theta = 60°$, $\Phi = 0°$ and $\Theta = 60°$, $\Phi = 180°$ are depicted in Fig. 8.19. Here F_0 is intensity of incident radiation. Solar light direction is shown by arrows. Calculation results for the same problem, performed by the Monte Carlo method (code MYSTIC) (Mayer, 1999), are presented in Fig. 8.19 as well. The difference between results, obtained by two different methods, is less than 1% in the areas far from the boundary and less than 4.5% near the boundary, where the exact solution possesses great gradients.

The constant value of brightness far from the boundary can be obtained based on the slab model. The code ROZ-6.5 (Averin et al., 1991), was used for transport problem calculations in the optically thin aerosol slab, whereas asymptotic formulas were applied for radiation obtaining in optically thick cloud. The difference between results, obtained via RADUGA-5.1(P) and 1D results is less than 1%. This fact confirms, that the boundary condition (8.31) properly imitates the semi-infinite medium.

Two imitations of really observable atmospheric phenomena can be seen in Fig. 8.19. These are the *cloud shadow* (minimum of light brightness in aerosol slab near $\Phi = 180°$) and *brightening* (brightness maximum in aerosol slab near $\Phi = 0°$). These two effects are primarily caused by the direct light transfer through a scattering medium. They are relevant not only in the case of a simple model of a semi-infinite homogeneous cloud but also for more general broken cloud systems. They demonstrate the influence of the vertical medium boundary on scattered radiation brightness near this boundary and can be used to study radiative edge effects of cloud optics (Kokhanovsky, 2006).

8.14 Simplified discrete ordinates models

8.14.1 Accuracy estimation for simple 1D models

The solution of inverse problem s and radiance balance calculations in climate models are currently carried out mainly by means of simple 1D models, where radiation transfer in horizontal directions is not taken into account. The plane-parallel slab model (PP) and the independent column approximation (ICA) belong to the class of 1D models. In the frames of the PP model a cloud is considered as horizontally homogeneous, whereas in the ICA a cloudy model is composed of large homogeneous parallelepipeds (pixels). In the framework of ICA the parallelepipeds can also possess a stratified structure. Such an approximation is also called Independent Pixel Approximation (IPA).

In last decade a great number of papers have studied the features and accuracy of these 1D models under a variety of atmospheric parameters. In our opinion, the main conclusion was formulated by Marshak and Davis (2005): 'It is time to think of 3D theory as the golden standard in atmospheric radiative transfer rather than a perturbation of standard 1D theory'. However, we mention here some results obtained via 1D models to complete the picture.

The capabilities of the ICA model were analyzed in problems of short-wave radiation propagation through deep convective clouds (Giuseppe and Thompkins, 2003) by means of the code SHDOM (Evans, 1998). It has been shown, that energy imbalance is mainly caused by two opposing effects: side illumination and shadowing (see Fig. 8.19). The comparison between ICA and PP models shows that for deep convective clouds geometry-related effects can have a larger influence on radiative transfer calculations than the internal optical inhomogeneities. Similar results were obtained for ultraviolet light transfer problems as well (Scheirer and Macke, 2003). The shortcomings of these investigations are indicated by Giuseppe and Thompkins (2003). They are due to the simplified model of the cloud structure. Hence, the characteristic radiative biases, obtained in the frames of the 1D models, cannot be applied to most real situations. The numerical experiment example and the results obtained are depicted in Table 8.1 and Figs 8.20 and 8.21.

Table 8.1. Reflectance, transmittance, and absorptance for IPA and PP biases for two numerical experiments (the solar zenith angle (SZA) is equal to 0 (SZA0) and 60 (SZA60) degrees) (after Guiseppe and Thompkins, 2003)

	IPA Bias SZA0		PP Bias SZA0		IPA Bias SZA60		PP Bias SZA60	
	Abs.	Rel.%	Abs.	Rel.%	Abs.	Rel.%	Abs.	Rel.%
Reflectance	0.016	16	−0.023	−19	0.013	8.6	−0.0095	−5.9
Transmittance	0.024	3.4	0.023	3.5	−0.018	−2.8	0.0082	1.3
Absorptance	−0.040	−23	0.0	0.0	0.0049	2.3	0.0013	0.63

Abs., absolute; Rel., relative.

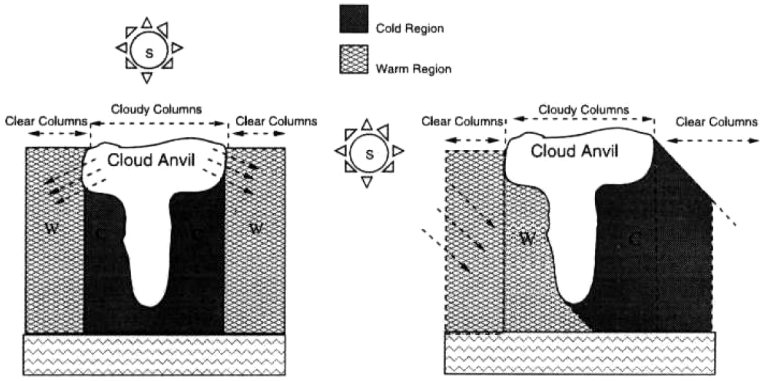

Fig. 8.20. Scheme of the redistribution of the radiation between clear and cloudy columns. The clear regions surrounding cloudy columns undergo an enhancement of fluxes with an associated warming (W, lighter shading) in the Sun-overhead case due to the 'spilling' of radiation from the cloud to the clear region and due to the horizontal transport of photons. The opposite happens when the Sun is set at degree zenith angle, with an increased role of shading (darker shading), while clear- sky heating rates on the sunny side of the cloud are enhanced (after Guiseppe and Thompkins, 2003).

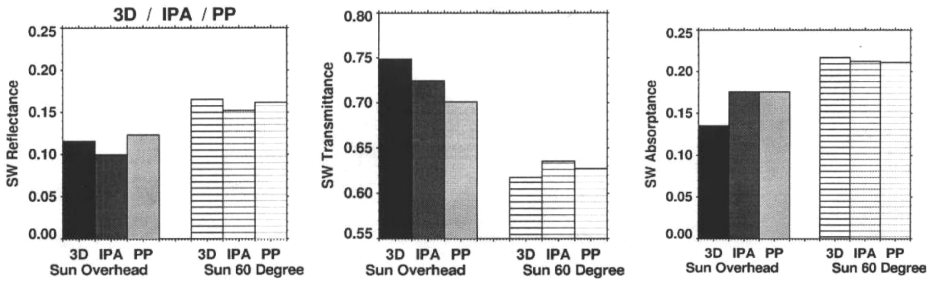

Fig. 8.21. Reflectance, transmittance, and absorptance for the two experiments SZA0 and SZA60. The calculation is performed for the whole domain using the full 3D radiative transfer, the independent pixel approximation (IPA), and plane-parallel (PP) methods (after Guiseppe and Thompkins, 2003).

Horizontal radiation transfer in clouds, modeled as inhomogeneous stratified columns, and its influence on cloud energy absorption was investigated by Titov (1998) for the case of lognormal particle distribution and the power law of energy spectrum of cloud depth. In addition, a realistic fractal cloud model was used. It was shown in the frames of the ICA model, that the contribution of the horizontal component to the full radiation field in clouds possesses the following features: (1) it is comparable with transmitted and absorbed radiation; (2) it is strongly dependent on cloud fractal structure and optical depth. The results allow us to conclude that in the majority of situations neglecting horizontal transport will lead to uncertainties in absorption estimations (anomalous absorption). Besides, not accounting for the horizontal transport will result in violation of the one-

to-one correspondence between optical and radiative pixel characteristics. Two possible ways of overcoming the difficulties mentioned are discussed in the paper.

The smoothness properties of radiation fields for stratified clouds, horizontal fluctuations of extinction, modeled via multiplicative cascades, were analyzed by Marshak and Davis (1995). As it turns out, the ICA model can be applied for sufficiently large pixels, whereas in the case of small pixels (i.e. pixel sizes less then 200–500 m) the ICA highly underestimates the liquid water variability in clouds.

A novel approach for 3D effect estimation and exclusion is proposed by Varnai and Marshak (2002). The method is based on satellite image analysis, that is to say, on the estimation of reflective cloudy brightness for visible and thermal infrared light. This technique makes it possible to decrease errors in the problem of cloud optical property reconstruction by means of ICA models, although the errors cannot be excluded completely. The necessity of 3D model introduction for processing reflected radiation fields, obtained in real measurements with high-resolution accuracy, has been also stressed by Marshak and Davis (1998).

Some final results of longstanding extended studies of 1D atmosphere models are presented in a detailed investigation by Barker et al. (2003). Here 1D and 3D model comparison was carried out in the frames of three test problems, typical for tropical atmosphere:

clear-sky – clouds and aerosol are absent, slab height is near 100 km.
CLOUD A – low cloudiness (a cloud is located between 3.5 and 4 km).
CLOUD B – high cloudiness (a cloud is located between 10.5 and 11 km).

The calculation accuracy of three parameters has been studied. These are

- α_p – top-of-atmosphere albedo,
- α_{atm} – atmospheric absorption,
- α_{sfc} – surface absorption.

3D calculations were performed by the Monte Carlo method by means of four different codes. Deviations in the obtained results were less than 2%.

Twenty-five codes carried out 1D calculations, the line-by-line model being realized in two of them. Obtained results essentially differ among themselves and strongly deviate from 3D results. In particular, 1D models underestimate the value α_{atm} on the average by 15–25 Wm^{-2}, independently of cloud presence, for the problem with the Sun at zenith. Errors in 1D calculations are usually about 10% and even more. An example of a top-of-atmosphere albedo calculation is presented in Fig. 8.22. These facts give the authors the opportunity to conclude that a new methodology of radiation field calculations in large-scale models is very necessary. New codes should be fast and operative.

Results obtained by Kokhanovsky (2003a, 2005) can be used in problems of algorithm development. A important case of 3D light scattering problems in a turbid medium layer is considered in these papers. It is shown that in the case of optically thick layer the statistical distributions for reflected, transmitted and absorbed radiation are related via simple analytical expressions with the statis-

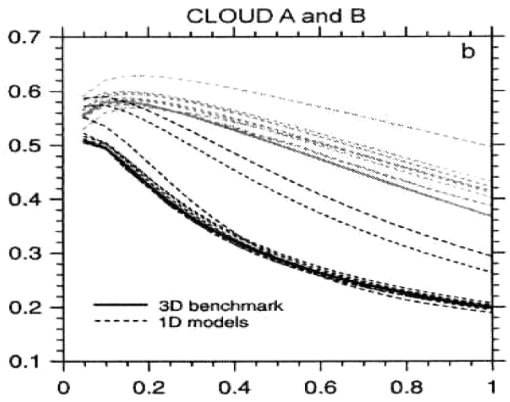

Fig. 8.22. Dashed lines represent broadband TOA albedos as a function of solar zenith angle cosines for the homogeneous CLOUD A (lighter lines) and CLOUD B (darker lines) predicted by all 1D codes assuming maximum/random overlap. Solid lines are corresponding values for one of the 3D MC codes (after Barker et al., 2003).

tical distribution of the optical thickness. These expressions may be applicable to both direct and inverse problem s of cloud optics.

8.14.2 Spherical atmosphere models

The 3D spherical coordinate system exactly corresponds to the terrestrial atmosphere geometry (see Fig. 8.23).

The transport equation in the spherical geometry is solved mainly by a Monte Carlo method. However, it is not always possible to use MC methods for atmospheric radiation field calculations (Ougolnikov, 1999) – because of large optical thickness of cloudy atmosphere. From this and other works we can see that grid spherical atmospheric models should be developed.

Currently algorithms, based on mesh schemes of the discrete ordinates method, are included in a small number of codes only. They use the charac-

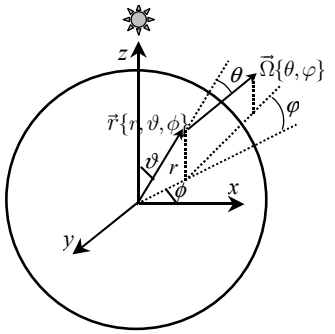

Fig. 8.23. 3D spherical coordinate system.

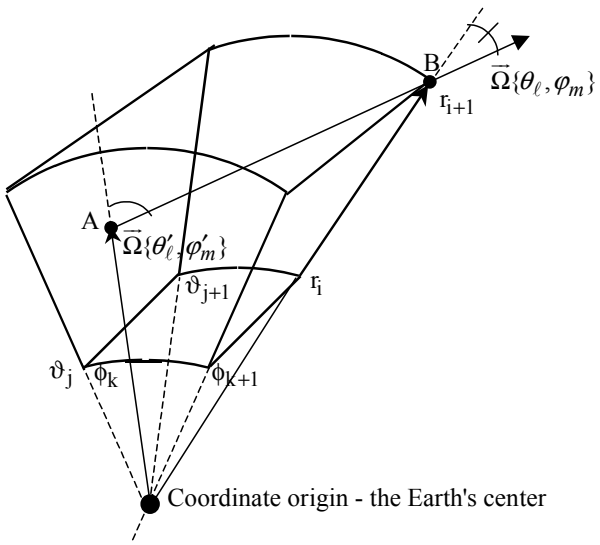

Fig. 8.24. Example of characteristics intersection scheme with a grid mesh in spherical coordinate system.

teristics method, where the transport equation is written in the integral form (see (8.18)). Integration in (8.18) is carried out along characteristics of the differential operator $\hat{L}$ (see Eq. (8.2)). An example of characteristics propagation through a curvilinear mesh in 3D spherical geometry is shown in Fig. 8.24, where

- AB – characteristics segment inside the mesh,
- r_i – grid node radii,
- ϑ_j – grid node latitudes,
- ϕ_k – grid node longitudes,
- $\vec{\Omega}\,(\theta_\ell, \varphi_m)$ – grid node angles of viewing.

Figure 8.24 demonstrates the main difficulty arising in solving the transport equation in spherical geometry: its own local coordinate system for viewing angles $\{\theta, \varphi\}$ is being used at each spatial point $\{r, \vartheta, \phi\}$, and so viewing angles in a local coordinate system are changing, when the viewing point is moved along characteristics (see points B and A).

Because the right-hand side of transport equation (8.1) depends on $\psi(\vec{r}, \vec{\Omega})$ (that is, on the solution sought for), the iterative process on successive scatterings is usually applied to calculate $\psi(\vec{r}, \vec{\Omega})$.

An example of the algorithm of the transport equation being solved in 3D spherical geometry is presented in the work of Emde (2005). It is given in detail the next section.

So-called 'limb' observations play an important role in atmospheric investigations. Their scheme is presented in Fig. 8.25, where θ_T and ϕ_T are zenith and azimuth solar angles respectively (Griffioen and Oikarinen, 2000). Now these

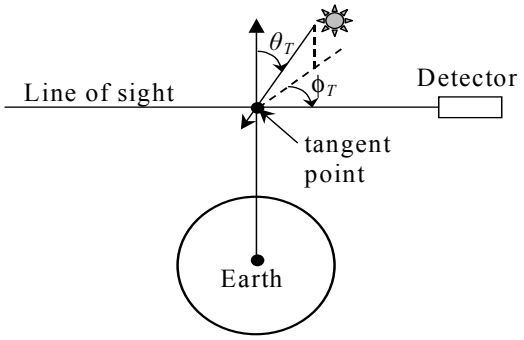

Fig. 8.25. 'Limb' observation scheme.

observations are performed by means of satellites for different spectral ranges. They permit

- detection of aerosol layers in the atmosphere,
- measurement of the temperature of the stratosphere, ozone concentration in the mesosphere and concentration of NO_2 in the stratosphere.

In the codes, which are intended for 'limb' observation treatments, the simplified combined models are used, because much time is required to solve the transport equation in 3D geometry.

These combined models are usually pseudo-spherical, because the scattering integral, defining multi-scattered radiation intensity, is calculated in the frames of the plane-parallel model. The examples are:

(a) model LIDORT (Linearized Discrete Ordinate Radiative Transfer) (Spurr, 2002);
(b) model LIMBTRAN (Griffioen and Oikarinen, 2000);
(c) model CDI (Combined Differential-Integral) (Rozanov et al., 2001), where light refraction is taking into account.

Besides, special spherical models are developed. Among them there is the model CDIPI (CDI Picard Iteration), based on characteristics method in combination with successive scattering order iterations. Here the initial approximation is calculated by means of the pseudo-spherical model CDI of Rozanov et al. (2000), refraction effects being taken into account.

The spherical model GSS (Gauss–Seidel Spherical) is intended for radiation intensity calculation in fixed desired radial directions (Herman et al., 1994). For the purpose a cone with a vertex in the Earth's center is constructed, the deviation angle between cone generatrix and the considered direction being equal to ϑ_0 (see Fig. 8.26). A grid over cone height with nodes $R_0 + r_i$, $i = 1, 2, \ldots$, where R_0 is the Earth's radius, is introduced inside the cone. The transport equation solution inside the cone is calculated via the characteristics method in the frames of 1D spherical model. To determine the radiation intensity, entering the cone, it is assumed that the ratio of multiply scattered to unscattered light

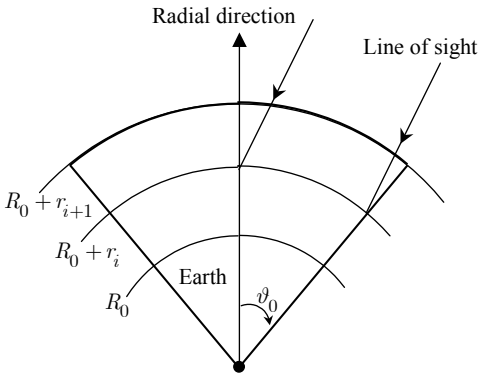

Fig. 8.26. Spatial grid and conical boundaries in the spherical model GSS.

intensity is constant over the atmospheric shell. A special iterative scheme has been constructed, taking into account both successive radiation scattering orders and boundary conditions. It provides a fast and accurate technique for finding the solution. Results of calculations obtained via both the MC method and other methods were used for model testing. The solutions obtained by the other grid methods were employed too. The interval of admissible angle ϑ_0 variation was found. The angles are between 0.25° and 2°. Detailed comparison of reflected and transmitted light intensity for spherical and plane-parallel atmospheres for different solar and viewing angles has been carried out. Reflection from the Earth was not taken into account. Numerous illustrations were prepared for 50-km atmosphere, the Earth's radius being assumed to be equal to 6380 km. Figure 8.27 given by the authors clearly demonstrates the influence of the sphericity of the Earth's atmosphere.

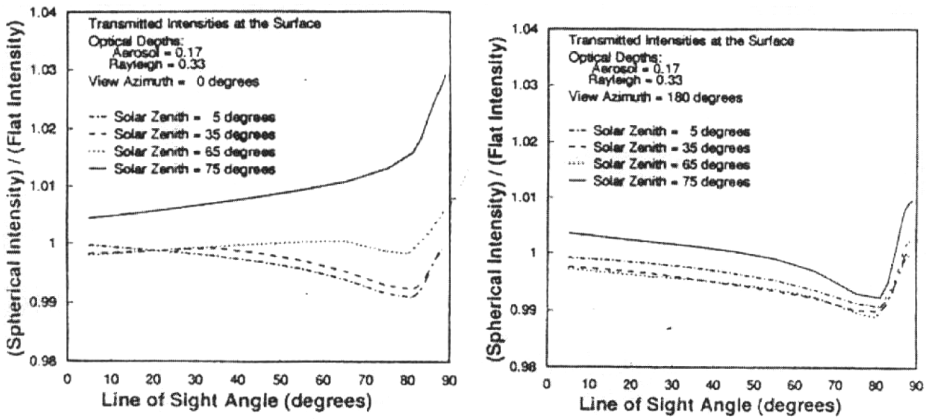

Fig. 8.27. Ratio of spherical- to flat-atmosphere transmitted intensities at the surface for a scattering atmosphere with a 0.50 optical depth. Left-view azimuth = 0 degrees, right −180 degrees (after Herman et al., 1994).

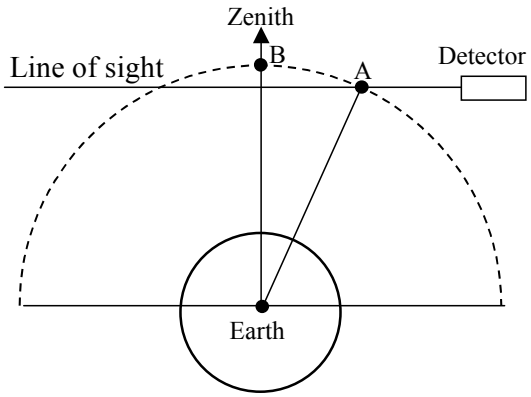

Fig. 8.28. Spherical model GSLS.

It should be noted that iterations over boundary conditions, being taken into account in the model, can be more easily performed both in (x, y) and in (x, y, z) geometries (see section 8.14). The boundary condition inclusion enables us to decrease the calculation time. However, a theoretical base for this inclusion is so far absent.

The spherical GSLS (Gauss–Seidel Limb Spherical) model of (Loughman et al., 2004) represents a more accurate and faster model than the GSS model (Herman et al., 1994, 1995). In the frames of the GSLS model, scattered radiation intensity in the line of sight is assumed to be equal to scattered radiation intensity at the point, which is characterized by the same coordinate r, but is located at the zenith radial direction. For example, the intensity value at the point A is equated to the intensity value at the point B (see Fig. 8.28). In addition polarization effects are also taken into account in the frames of GSLS model.

Finally, note that in some special cases the transport equation solution in 1D spherical geometry can be defined as the solution of the same equation in plane-parallel geometry under special boundary conditions (El-Wakil et al., 2001; Yildiz, 2002). This enables the use of analytical methods, developed for the plane-parallel transport problems, to obtain special solution classes for transport problems with spherical geometry. It can be important when one deals with inverse transport problems.

The paper by Loughman et al. (2004), is devoted to the investigation and comparison of six atmospheric models. In two of the models the MC method was used, whereas four models were based on DOM. These are the CDI, GSLS, LIMBTRAN and CDIPI models (see above). The detailed numerical analysis of these models has been carried out, including:

- comparison of results for test problems, obtained via different models;
- comparison of computational speeds;
- estimation of the accuracy of various techniques.

A solution qualified as an exact one if the calculation results obtained via two different MC codes provided a difference in the results smaller than 1–2%.

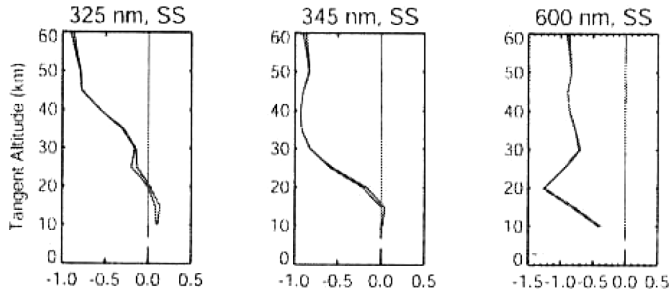

Fig. 8.29. Comparison between the vector RT models (left-hand two lines: GSLS and MC++ (Postylyakov, 2004)). Calculations were performed for an aerosol-free atmosphere, the underlying surface albedo equal to zero and for the same viewing geometry as in Figs. 8.21, 8.25. Right-hand vertical line corresponds to the calculations according to the scalar RT theory. The figures present percent differences for the exact SS (single scattering) source function from the case when the polarization is neglected (after Loughman et al., 2004).

As the comparison shows, the DOM codes mentioned provided low accuracy in situations where the optical path between calculation and detector points was great or when the zenith viewing angle changed significantly along the line of sight. The comparison of calculations according different radiative transfer models is presented in Fig. 8.29.

8.14.3 DOM in problems with polarization

Light polarization arises mainly owing to single scattering of photons by water droplets, aerosol particles, ice crystals or air molecules. Multiple scattering processes lead to the decrease of the light polarization degree and increase the entropy of the radiation field (Kokhanovsky, 2003b; Hovenier and Domke, 2005; Mishchenko et al., 2006).

The retrieval of microscopic and macroscopic properties of clouds is based often on the measurements of the polarization characteristics of the scattered light. Hence, in many cases polarization effects should be taken into account in atmospheric optics problems. In this section we provide a brief description of some models on polarized radiation transfer that rely on the Vector Radiation Transport Equation (VRTE).

In these models four unknown functions, forming the so-called Stokes vector $S(I, Q, U, V)$, contain full information of light beam intensity, degree of polarization and polarization form.

1. In a paper of Rozanov and Kokhanovsky (2006) the algorithms of the VRTE solution based on the discrete-ordinates technique (DOT) (Siewert, 2000) is presented. A new code SCIAPOL_1.0 for the solution of the VRTE for the Stokes vector in a plane-parallel turbid slab, illuminated by the monodirected wide beam, is described. The phase matrix is presented in the form of a decomposition into series on associated Legendre functions.

The code can be applied to the solving of direct and inverse problem s of atmospheric optics, including analysis of the applicability of scalar approximation in complicated light transfer problems in media containing molecular atmosphere, aerosols and clouds. Some new approximations for the calculation of reflection function and light polarization degree under unpolarized light illumination conditions are proposed. Code capabilities have been demonstrated in a number of real physical problems. In particular, comparison of scalar and vector intensity approaches has been carried out.

2. The DOIT (Discrete Ordinate Iterative) algorithm of the polarized radiation field calculation in 1D and 3D spherical geometries is presented in the work of Emde (2005). It relies on the numerical solution of the transport equation for Stokes parameters by the characteristics method, the iterative successive-orders-of-scattering method being applied.

The main equations of the algorithm provide solution values corresponding to grid meshes so that the solution values can be immediately compared with satellite measurements in 'limb' geometry (zenith angle $\theta_{\ell\mathrm{imb}}$), in geometry 'down viewing' (angle θ_{down}) and in geometry 'up viewing' (angle θ_{up}) (see Fig. 8.30). Note, that scattered light intensity is much larger in the 'limb' geometry, than in the geometry 'down viewing' due to a larger optical path along the line of sight. So, the 'limb' measurements are more useful from the viewpoint of cloud optical property reconstruction.

The influence of particle size and orientation on light polarization was studied in the framework of these models. It was established that for clouds with horizontally oriented particles the polarization accounting significantly changes light intensity. Therefore, in many cases polarization effects should be taken into account, even if it is necessary to calculate only light intensity. The issue of calculation time is of importance, as usual. The time greatly increases as cloud size increases. For example, calculation of a thin cloud via a 3D model for the four-component Stokes vector with the help of a 3 Ghz Pentium 4 takes 50 min. The same calculation of the two-component Stokes vector takes 37 min. Complete calculation of a similar thick cloud takes 150 min.

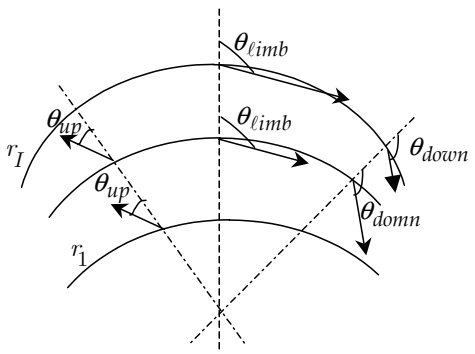

Fig. 8.30. Observation schemes.

The calculation via a 1D model requires less time. Full calculation of the thick cloud via a 1D model requires 30 sec. Therefore, 3D models cannot be so far used in operational or 'line-by-line' calculations.

3. The linearized MCC++ spherically symmetric 2D model is presented in the paper of Postylyakov (2004). It is intended for radiation field calculations at a large number of wavelengths by the Monte Carlo method. The technique is based on calculation of radiative functionals for radiation transfer problems with a single wavelength (that is the linearization point for the transport equation). These functionals and their derivatives are necessary for the solving of atmosphere optics inverse problem s. The MCC++ model takes into account aerosol and molecular scattering, gaseous and aerosol absorption and radiation reflection by a boundary surface according to the Lambert law.

8.15 Conclusion

Radiation propagation through a horizontally and vertically inhomogeneous atmosphere is usually described by the transport equation. To solve this equation either statistical algorithms (Monte Carlo), or grid methods, in particular the discrete ordinates methods, are used.

The Monte Carlo methods rely on direct modelling of random photon paths. They allow us to take into account the arbitrarily complicated structure of a calculation region. But they require large time expenditure for transport problems with optically thick media, where great numbers of trajectories should be calculated to guarantee high accuracy of results.

The chapter is aimed at the description of the discrete ordinates method, intended for multi-dimensional transport equation solving. The representation of the transport equation coefficients, grid constructions and grid scheme developments are considered in detail. In addition, long characteristics schemes that are frequently used for solving of atmospheric optics problems, and the other types of schemes, that are currently successfully exploited both in model radiation transfer problems and in applications, are also considered and discussed. Particular attention is focused on the accuracy of the schemes and their capabilities in the calculation of smooth solutions in homogeneous media and quickly varied solutions in strongly heterogeneous regions. In the latter case grid solutions can be distorted by non-physical oscillations of large amplitude, if only special approaches are not applied to reduce or eliminate the oscillations.

Different iterative algorithms for solving grid equations are considered. The popular successive-orders-of-scattering method converges fairly slowly (especially in the case of optically thick and weakly absorbing media). So, the main types of convergence acceleration method are described.

Methods of grid algorithm parallelizing are presented as well, and the conditions of their effectiveness are considered.

The main characteristics of two codes for solving 3D radiation transport problems in the atmosphere by the discrete ordinates method are described. These are SHDOM and RADUGA-5.1(P).

Simplified models are also presented, which permit the reducing of the scope of calculations for radiation transport problems that account for the 'limb' model of the atmosphere. The features of the simplified ICA model, which neglects horizontal radiation transfer, are discussed. In particular, the issue of the accuracy of medium optical characteristics retrieval via using a radiation transport model, neglecting horizontal radiation transfer, is also discussed.

The described grid methods, which were previously used mainly in different neutron transport problems, will be also useful in light scattering media optics, especially if the radiation field in turbid media having complex geometrical shapes is of interest.

References

Adams, M.L., 1991: A new transport discretization scheme for arbitrary spatial mesh in (x, y) geometry, *Proc. of Int. Top. Meeting Advances Mathematics, Computations and Reactor Physics, Pittsburg, USA, April 28 – May 2, 1991*, Vol. 3, 13.2.2–1 – 13.2.2–9.

Adams, M.L., Larsen, E.W., 2002: Fast iterative methods for discrete-ordinates particle transport calculations, *Progress in Nuclear Energy*, **40**, 3–159.

Aussourd, Ch., 2003: A TN adaptive ray effect mitigation for styx 3D, *Proc. of Joint Int. Conf. on Supercomputing in Nuclear Applications, Paris, France, September 22–24*, 2003, CD.

Averin, A.V., Voloschenko, A.M., et al., 1991: The ROZ–6.4 one–dimensional discrete ordinates neutrons, gamma–rays and charged particles transport code, *Proc. of Int. Top. Meeting Advances Mathematics, Computations and Reactor Physics, Pittsburg, USA, April 28 – May 2, 1991*, Vol. 5, 30.3.5–1 – 30.3.5–4.

Azmy, Y.Y., 1988a: The weighted diamond-difference form of nodal transport methods, *Nucl. Sci. Eng.*, **98**, 29–40.

Azmy, Y.Y., 1988b: Multidimensional nodal transport methods for multi-instruction and multi-data distributed memory machine, *Trans. Am. Nucl. Soc.*, **56**, 292.

Azmy, Y.Y., 1992: Arbitrary high order characteristic method for solving the neutron transport equation, *Ann. Nucl. Energy*, **19**, 593–606.

Badruzzaman, A., 1985: An efficient algorithm for nodal transport solution in multi-dimensional geometry, *Nucl. Sci. Eng.*, **89**, 281–290.

Baker, R.S., Asano, C.A., Shirley, D.N., 1995: Implementation of the first order form of the 3D discrete ordinate equations on T3D, *Trans. Am. Nucl. Soc.*, **73**, 170.

Barbucci, P., Pasquantonio D.Di, 1977: Exponential supplementary equations for Sn methods: The one–dimensional case, *Nucl. Sci. Eng.*, **63**, 179–187.

Barker, H.W. et al., 2003: Assessing 1D atmospheric solar radiative transfer models: Interpretation and handling of unresolved clouds, *J. Climate*, **16**, 2676-2699.

Bass, L.P., Voloschenko, A.M., Germogenova, T.A., 1986: *Discrete ordinates techniques in problems of radiative transfer*, Keldysh Institute of Applied Mathematics, Moscow (in Russian).

Bass, L.P., Nikolaeva, O.V., 1997: Correct calculation of angular flux distributions in strongly heterogeneous media and voids, *Proc. of Joint Int. Conf. on Mathematical Methods and Supercomputing for Nuclear Applications, Saratoga Springs, October 5–9, 1997*, Vol. 2, 995–1004.

Cahalan, R.F., Oreopoulos, L., et al., 2005: I3RC. Bringing together the most advanced radiative transfer tools for cloudy atmospheres, *Bull. Amer. Meteor. Soc.*, September 2005, 1275–1293.

Carlson, B.G., 1976: A method of characteristics and other improvements in solutions methods for the transport equations, *Nucl. Sci. Eng.*, **61**, 408–425.

Castriani, Ch.L., Adams, M.L., 1995: A nonlinear corner balance spatial discretization for transport on arbitrary grids, *Proc. of Int. Conf. Mathematics and Computations, Reactor Physics, and Environmental Analyses, Portland, USA, April 30 – May 4, 1995*, Vol. 2, 916–927.

Chandrasekhar, S., 1950: *Radiative transfer*, Oxford University Press, Oxford.

Dahmani, M., Chavez-Guzman, J., Roy, R., Koclas, J., 2003: Data management in parallel transport calculation, *Proc. of Joint Int. Conf. on Supercomputing in Nuclear Applications, Paris, France, September, 22–24*, 2003, CD.

Dorr, M.R., Salo, E.M., 1995: Performance of a neutron transport code with full phase space decomposition on the Cray research T3D, *Proc. of Int. Conf. Mathematics and Computations, Reactor Physics, and Environmental Analyses, Portland, USA, April 30 – May 4, 1995*, Vol. 2, 1535–1544.

Elsawi, M.A., Abdurrahman, N.M., Azmy, Y.Y., 2003: Asymptotic analysis of the spatial weights of the arbitrarily high order transport method of the characteristic type, *Proc. of Int. Conf. Nuclear Mathematical and Computational Sciences, Tennessee, April 6–11*, 2003, CD.

El-Wakil, S.A., et al., 2001: Radiative transfer in a spherical medium, *J. Quant. Spectrosc. Radiat. Transfer*, **69**, 49-59.

Emde, C., 2005: A polarized discrete ordinate scattering model for radiative transfer simulations in spherical atmospheres with thermal source. PhD thesis, University of Bremen, Bremen.

Evans, K.F., 1998: The spherical harmonics discrete ordinate method for three–dimensional atmospheric radiative transfer, *J. Atmos. Sci.*, **55**, 429–446.

Fischer, J.W., Azmy, Y.Y., 2003: Parallel performance of the angular versus spatial domain decomposition for discrete ordinate method, *Proc. of Joint Int. Conf. on Supercomputing in Nuclear Applications, Paris, France, September, 22–24*, 2003, CD.

Germogenova, T.A., 1985: *Local properties of transport equation solutions*, Nauka, Moscow (in Russian).

Giuseppe, F.Di., Thompkins, A.M., 2003: Three-dimensional radiative transfer in tropical deep convective clouds, *J. Geophys. Res.*, **108**, 10.1029/2003JD003392.

Griffioen, E., Oikarinen, L., 2000: LIMBTRAN: A pseudo three-dimensional radiative transfer model for the limb-viewing imager OSIRIS on the ODIN satellite, *J. Geophys. Res.*, **105**, 29,717 – 29,730.

Grove R.E., Pevey R.E., 1995: A characterictics based multiple balance approach for SN on arbitrary polygonal grids, *Proc. of Int. Conf. Mathematics and Computations, Reactor Physics, and Environmental Analyses, Portland, USA, April 30 – May 4, 1995*, 928–937.

Haghighat, A., Azmy, Y.Y., 1991: Parallelization of a spherical Sn algorithm based on the spatial domain decomposition, *Proc. of Int. Top. Meeting Advances Mathematics, Computations and Reactor Physics, Pittsburg, USA, April 28 – May 2, 1991*, 1.1.3.-1. – 1.1.3.-12.

Hanebutte, U.R., Lewis, E.E., 1991: A discrete ordinate response matrix method for massively parallel computers, *Proc. of Int. Top. Meeting Advances Mathematics, Computations and Reactor Physics, Pittsburg, USA, April 28 – May 2, 1991*, 1.1.1-1. – 1.1.1.-10.

Hennart, L.P., del Valle, E., 1997: New nodal element schemes for the discrete ordinates transport equation, *Proc. of Joint Int. Conf. on Mathematical Methods and Supercomputing for Nuclear Applications, Saratoga Springs, October 5–9, 1997*, Vol. 1, 19–28.

Herman, B.M. et al., 1994: Numerical techniques for solving the radiative transfer equation for a spherical shell atmosphere, *Appl. Opt.*, **33**, 1760-1770.

Herman, B.M. et al., 1995: Comparison of the Gauss-Seidel spherical polarized radiative transfer code with other radiative transfer codes, *Appl. Opt.*, **34**, 4563–4572.

Hovenier, J., Domke, H., 2005: *Transfer of polarized light in planetary atmospheres. Basic concept and practical methods*, Springer, Berlin.

Koch, R., Krebs, W., Wittig, S., Viskanta, R., 1995: Discrete ordinates quadrature schemes for multidimensional radiative transfer, *J. Quant. Spectrosc. Radiat. Transfer*, **53**, 353–372.

Kokhanovsky, A.A., 2003a: The influence of horizontal inhomogeneity on radiative characteristics of clouds: an asymptotic case study, *IEEE Trans. Geosci. Remote Sensing.*, **41**, 817–825.

Kokhanovsky, A.A., 2003b: *Polarization optics of random media*, Springer, Berlin.

Kokhanovsky, A.A., 2005: Statistical properties of light reflected and transmitted by a thick horizontally inhomogeneous turbid layer, *J. Opt. Soc. Am. A.*, **22**, 2419–2423.

Kokhanovsky, A.A., 2006: *Cloud Optics*, Springer, Dordrecht.

Landesman, M., Morel, J.E., 1989: Angular Fokker–Planck decomposition and representation techniques, *Nucl. Sci. Eng.*, **103**, 1–11.

Lathrop, K.D., 1969: Spatial differencing of the transport equation: positivity vs. accuracy, *J. Comp. Phys.*, **4**, 475–490.

Lebedev, V.I., 1976. On quadratures on spheres. *Computational Mathematics and Mathematical Physics*, **16**, 293-307.

Longoni, G., Haghighat, A., 2001: Development of new quadrature sets with the 'ordinate splitting' technique, *Proc. of Int. Meeting on Mathematical Methods For Nuclear Application, Salt Lake City, Utah, September, 2001*, CD.

Loughman, R.P., Griffioen, E., Oikarinen, L., Postylyakov, O.V., Rozanov, A., Flittner, D.E., Rault, D.F., 2004: Comparison of radiative transfer models for limb-viewing scattering sunlight measurements, *J. Geophys. Res.*, **109**, 10.1029/2003JD003854.

Madsen, N.K., 1975: Spatial convergence properties of the diamond difference method in x, y geometry, *Nucl. Sci. Eng.*, **12**, 164–176.

Marchuk, G.I., et al.,: 1980: *The Monte Carlo methods in atmospheric optics*, Springer, Berlin.

Marchuk, G.I., Lebedev, V.I., 1981: *Numerical methods in neutron transport theory*, Atomizdat, Moscow (in Russian).

Marshak, A., Davis, A., et al., 1995: Radiative smoothing in fractal clouds. *J. Geophys. Res.*, **100**, 26,247 – 26,261.

Marshak, A., Davis, A., et al., 1998: Radiative effects of sub-mean-free-path liquid water variability observed in stratiform clouds, *J. Geophys. Res.*, **103**, 19557-19567.

Marshak, A., Davis, A., 2005: *Three-dimensional radiative transfer in cloudy atmospheres, Springer*, Berlin.

Mathews, K.A., Minor, B.M., 1991: Step adaptive characteristic spatial quadrature in two-dimensional Cartesian coordinates, *Proc. of Int. Top. Meeting Advances Mathematics, Computations and Reactor Physics, Pittsburg, USA, April 28 – May 2, 1991*, Vol. 3, 13.2.4–1 – 13.2.4–12.

Mathews, K.A., Minor, B.M., 1993: Adaptive characteristic spatial quadratures for discrete ordinates neutral particle transport – the rectangular cell case, *Transport Theory Stat. Phys.*, **22**, 655–685.

Mathews, K.A., 1999: On the propagation of rays in discrete ordinates, *Nucl. Sci. Eng.*, **132**, 155–180.

Mayer, B., 1999: I3RC phase 1 results from the MYSTIC Monte Carlo model, *Proc. of I3RC Workshop, Tucson, Arizona, November 17–19, 1999.*

Mishchenko, M.I., Travis L.D., Lacis, A.A., 2006: *Multiple scattering of light by particles: radiative transfer and coherent backscattering*, Cambridge University Press, Cambridge.

Morel, J.E., Larsen, E.W., 1990: A multiple balance approach for differencing the Sn equations, *Nucl. Sci. Eng.*, **105**, 1–15.

Morel, J.E., Manteuffel, T.A., 1991: An angular multigrid acceleration technique for Sn equations with highly forward-peaked scattering, *Nucl. Sci. Eng.*, **107**, 330–342.

Morel, J.E., Dendy Jr, J.E., Wareing, T.A., 1993: Diffusion–accelerated solution of the two–dimensional Sn equations with bilinear-discontinuous difference, *Nucl. Sci. Eng.*, **115**, 304–319.

Morel, J.E., 2005: Basic Krylov methods with application to transport, *Proc. of Int. Conf. on Mathematics and Computation, Supercomptuting, Reactor Physics and Nuclear Biological Applications, Avignon, France, September 12–15, 2005*, CD.

Nikolaeva, O.V., 2004: Special grid approximations for the transport equation in strongly heterogeneous media with the (x, y)-geometry, *Computational Mathematics and Mathematical Physics*, **44**, 835–854.

Nikolaeva, O.V., Bass, L.P., Germogenova, T.A., Kokhanovsky, A.A., Kuznetsov, V.S., Mayer, B., 2005a: The influence of neighbouring clouds on the clear sky reflectance studied with the 3-D transport code RADUGA, *J. Quant. Spectrosc. Radiat. Transfer*, **94**, 405-424.

Nikolaeva, O.V., Germogenova, T.A., Bass, L.P., Kuznetsov, V.S., 2005b: The discrete ordinates methods development to the transport equation solving. The 3D code Raduga-5.1 and multiprocessors computers, *Proc. of 19th International Conference on Transport Theory, Budapest, Hungary, July 24–29, 2005*, 115–117.

Nowak, P.F., Nemanic, M.K., 1999: Radiation transport calculation on unstructured grids using spatially decomposed and threaded algorithm, *Proc. of Int. Conf. Mathematics and Computation, Reactor Physics and Environmental Analysis in Nuclear Application, Madrid, Spain, September 27–30, 1999*, Vol. 1, 379–390.

Ougolnikov, O.S., 1999: Twilight sky photometry and polarimetry: The problem of multiple scattering at the twilight time, *Cosmic Res.*, **37**, 159–165.

Patchimpattapong, A., Haghighat, A., 2003: Testing an expert system for selection of mesh and decomposition on parallel Sn method, *Proc. of Int. Conf. Nuclear Mathematical and Computational Sciences, Tennessee, April 6–11, 2003*, CD.

Pautz, S.D., Morel, J.E., 1999: An angular multigrid acceleration method for SN equations with highly forward-peaked scattering, *Proc. of Int. Conf. Mathematics and Computation, Reactor Physics and Environmental Analysis in Nuclear Application, Madrid, Spain, September 27–30, 1999*, Vol. 1, 647–656.

Pautz, S.D., 2001: An algorithm for parallel Sn sweep on unstructured mesh, *Proc. of Int. Meeting on Mathematical Methods For Nuclear Application, Salt Lake City, Utah, September, 2001*, CD.

Petrovic, B., Haghighat, A., 1996: New directional theta–weighed SN differencing scheme and its application to pressure vessel fluence calculations, *Proc. of*

Radiation Protection and Shielding Topical Meeting, Falmouth, MA, Vol. 1, 3–10.

Postma, T., Viujic, J., 1999: The method of characteristics in general geometry with anisotropic scattering, *Proc. of Int. Conf. Mathematics and Computation, Reactor Physics and Environmental Analysis in Nuclear Application, Madrid, Spain, September 27–30, 1999*, Vol. 2, 1215–1224.

Postylyakov, O.V., 2004: Linearized vector radiative transfer model MCC++ for spherical atmosphere, *J. Quant. Spectrosc. Radiat. Transfer*, **88**, 297–317.

Rhoades, W.A., Engle, W.W., 1977: A new weighted-diamond formulation for discrete ordinates calculations, *Trans. Am. Nucl. Soc.*, **27**, 776–777.

Rozanov, A., Rozanov, V., Burrows, J.P., 2000: Combined differential-integral approach for the radiation field computation in a spherical shell atmosphere: non-limb geometry, *J. Geophys. Res.*, **105**, 22937–22942.

Rozanov, A., Rozanov, V., Burrows, J.P., 2001: A numerical radiative transfer model for a spherical planetary atmosphere: combined differential-integral approach involving the Picard iterative approximation, *J. Quant. Spectrosc. Radiat. Transfer*, **69**, 491–512.

Rozanov V.V., Kokhanovsky, A.A., 2006: The solution of the vector radiative transfer equation using the discrete ordinates technique: Selected applications, *Atm. Res.*, **79**, 241–265.

Ryzik, I.M., Gradstein, I.S., 1972: *Tables of integrals, series and products*, Academy Press, New York.

Samarsky, A.A., 1989: *Theory of difference schemes*. Nauka, Moscow (in Russian).

Sanchez, R., McCormic, N.J., 2004: Discrete ordinates solutions for highly forward peaked scattering, *Nucl. Sci. Eng.*, **147**, 249–274.

Santandrea, S., Sanchez, R., 2002: Positive linear and nonlinear surface characteristic scheme for the neutron transport equation in unstructured geometries, *Proc. of Physor-2002*, CD.

Scheirer, R., Macke, A., 2003: Cloud inhomogeneity and broadband solar fluxes, *J. Geophys. Res.*, **108**, 1029/2002JD003321.

Shwetsov, A.V., 1997: Solving the x–y geometry transport equation by linear discontinuous scheme with consistent flux correction, *Proc. of Joint Int. Conf. on Mathematical Methods and Supercomputing for Nuclear Applications, Saratoga Springs, October 5–9, 1997*, Vol. 2, 1487–1496.

Sjoden, G.E., Haghighat, A., 1997: Pentran-A-3D cartesian parallel Sn code with angular, energy, and spatial decomposition, *Proc. of Joint Int. Conf. on Mathematical Methods and Supercomputing for Nuclear Applications, Saratoga Springs, October 5–9, 1997*, Vol. 1, 553-562.

Siewert, C.E., 2000: A discrete-ordinates solution for radiative-transfer models that include polarization effects, *J. Quant. Spectrosc. Radiat. Transfer*, **64**, 227–254.

Spurr, R.J.D., 2002: Simultaneous derivation of intensities and weighting functions in a general pseudo-spherical discrete ordinate radiative transfer treatment, *J. Quant. Spectrosc. Radiat. Transfer*, **75**, 129–175.

Sushkevich, T.A., Strelkov, S.A., Ioltuhovsky, A.A., 1990: *Characteristic method in atmospheric optics*, Nauka Publishers, Moscow (in Russian).

Sushkevich, T.A., 2005: *Mathematical models of radiation transfer*, Moscow (in Russian).

Suslov, I.R., 1988: Characteristics method in region with complicated geometry, *Atomic energy*, **65**, 57–58 (in Russian).

Suslov, I.R., Pevey, R.E., 1997: Application of the quasi-stationary derivatives principle in transport theory, *Trans. Am. Soc.*, **76**, 214.

Takeda, T., Yamamoto, T., 2001: Nodal transport methods for XYZ and hexagonal-Z geometry, *Transport Theory Stat. Phys.*, **30**, 401–420.

Titov, G.A., 1998: Radiative Horizontal transport and absorption in stratocumulus clouds, *J. Atmos. Sci.*, **55**, 2549–2560.

Ullo, J.J., Dorning, J.J., Dodds, H.L., Pevey, R.E., 1982: A comparison of nodal transport methods based on exponential and polynomial expansions, *Trans. Am. Nucl. Soc.*, **43**, 367–369.

del Valle, E., Alonso, G., 2001: Exponential weakly-discontinuous nodal scheme for the transport equation, *Trans. Am. Nucl. Soc.*, CD.

Varnai, T., Marshak, A., 2002: Observations of three-dimensional radiative effects that influence MODIS cloud optical thickness retrievals, *J. Atmos. Sci.*, **59**, 1607–1618.

Vladimirov, V.S., 1958: Numerical solution of kinetic equation for sphere, *Trans. 'Computing mathematics'*, **3**, 3–33 (in Russian).

Voloschenko, A.M., 1981: Transport equation solving by the DSn method in heterogeneous media. Part 2. One-dimensional spherical and cylindrical geometries, in collection *'Numerical solution of the transport equation for one-dimensional problems'*, Keldysh Institute of Applied Mathematics, 64–91 (in Russian).

Voloschenko, A.M., Germogenova, T.A., 1994: Numerical solution of the time-dependent transport equation with pulsed sources, *Transport Theory Stat. Phys.*, **23**, 845–869.

Voloschenko, A.M., 1997: Geometrical interpretation of family of weighted nodal schemes and adaptive positive approximations for transport equations, *Proc. of Joint Int. Conf. on Mathematical Methods and Supercomputing for Nuclear Applications, Saratoga Springs, New York, October 5–9, 1997*, Vol. 2, 1517–1526.

Voronkov, A.V., Sychugova, E.P., 1997: Analysis of a class of characteristic methods for solving the transport equation in x–y and x–y–z geometry, *Proc. of Joint Int. Conf. on Mathematical Methods and Supercomputing for Nuclear Applications, Saratoga Springs, New York, October 5–9, 1997*, Vol. 2, 985–994.

Walters, W.F., 1982: Recent development in nodal and characteristic method in transport theory, *Trans. Am. Nucl. Soc.*, **43**, 611–612.

Walters, W.F., 1986: Augmented weighted-diamond form of the linear-nodal scheme of Cartesian coordinate systems, *Nucl. Sci. Eng.*, **92**, 192–196.

Walters, W.F., Wareing, T.A., Marr, D.R., 1995: The nonlinear characteristic scheme for (x, y) geometry transport problems, *Proc. of Int. Conf. Mathematics and Computations, Reactor Physics, and Environmental Analyses, Portland, USA, April 30 – May 4, 1995*, 340–348.

Wareing, T.A., 1997: An exponential discontinuous scheme for discrete–ordinate calculation in Cartesian geometries, *Proc. of Joint Int. Conf. on Mathematical Methods and Supercomputing for Nuclear Applications, Saratoga Springs, October 5–9, 1997*, Vol. 2, 1257–1266.

Warin, X., 1996: Recent results about Sn nodal method in neutron transport. *Proc. of Int. Conf. 3-D Deterministic Radiation Transport Computer Programs: Features, Applications and Perspectives, Paris, France, December 2–3, 1996*. 325–337.

Wiscombe, W., 1977: The delta-M method: Rapid yet accurate radiative flux calculations for strongly asymmetric phase functions, *J. Atmos. Sci.*, **34**, 1408–1422.

Yildiz, C., 2002: The FN solution of the time-dependent neutron transport equation for a sphere with forward scattering, *J. Quant. Spectrosc. Radiat. Transfer*, **74**, 521–529.

Zhougsheng, Xie, Xuehua, Zhy, Honghun, Wu., 1994: Two–dimensional discrete nodal transport method for solving neutron transport problems in curvilinear coordinates, *Proc. of the Int. Conf. on Reactor Physics and Reactor Computations, Tel–Aviv, Israel, January 23–26, 1994*, Vol. 3, 688–694.

Zmijarevic, I., 1999: Multidimensional discrete ordinate nodal and characteristics methods for the Apollo2 code, *Proc. of Int. Conf. Mathematics and Computation, Reactor Physics and Environmental Analysis in Nuclear Application, Madrid, Spain, September 27–30, 1999*, Vol. 2, 1587–1597.